Paleoproterozoic juvenile magmatism within the northeastern sector of the São Francisco paleocontinent: Insights from the shoshonitic high Ba-Sr Montezuma granitoids

Samuel Moreira Bersan, Alice Fernanda de Oliveira Costa, André Danderfer Filho, Francisco Robério de Abreu, Cristiano Lana, Glaucia Queiroga, Craig Storey, Hugo Moreira

PII: S1674-9871(20)30041-4

DOI: https://doi.org/10.1016/j.gsf.2020.01.017

Reference: GSF 950

To appear in: *Geoscience Frontiers*

Received Date: 26 June 2019

Revised Date: 8 December 2019

Accepted Date: 26 January 2020

Paleoproterozoic juvenile magmatism within the northeastern sector of the São Francisco paleocontinent: Insights from the shoshonitic high Ba-Sr Montezuma granitoids.

Samuel Moreira Bersan[a,d*], Alice Fernanda de Oliveira Costa[b], André Danderfer Filho[b], Francisco Robério de Abreu[c], Cristiano Lana[b], Glaucia Queiroga[b], Craig Storey[d], Hugo Moreira[d]

[a]Universidade Federal de Ouro Preto, Programa de Pós-graduação, Departamento de Geologia, Campus Morro do Cruzeiro, Ouro Preto, MG CEP 35400-000, Brasil.

[b]Universidade Federal de Ouro Preto, Departamento de Geologia, Campus Morro do Cruzeiro, Ouro Preto, MG CEP 35400-000, Brasil.

[c]Sustain Geologia Ltda. Teresa M. Valadares 503/502, Belo Horizonte, MG. CEP 30575-160, Brasil.

[d]University of Portsmouth, School of Earth and Environmental Sciences, Burnaby Building, Burnaby Road, Portsmouth, PO1 3QL, UK

* Corresponding author. E-mail address: samuelbersan@gmail.com (S. Bersan).

Abstract

New, integrated petrographic, mineral chemistry, whole rock geochemical, zircon and titanite U-Pb geochronology, and zircon Hf isotopic data from the Montezuma granitoids, as well as new lithogeochemical results for its host rocks represented by the Corrego Tingui Complex, provides new insights into the late- to post-collisional evolution of the northeastern São Francisco paleocontinent. U-Pb zircon dates from the Montezuma granitoids spread along the Concordia between ca. 2.2 Ga to 1.8 Ga and comprise distinct groups. Group I have crystallization ages between ca. 2.15 Ga and 2.05 Ga and are interpreted as inherited grains. Group II zircon dates vary from 2.04 Ga to 1.9 Ga and corresponds to the crystallization of the Montezuma granitoids, which were constrained at ca. 2.03 Ga by the titanite U-Pb age. Inverse age zoning is common within the ca. 1.8 Ga Group III zircon ages, being related to fluid isotopic re-setting during the Espinhaco rifiting event. Zircon $\varepsilon_{\mathrm{Hf}}(t)$ analysis show dominantly positive values for both Group I (–4 to +9) and II (–3 to +8) zircons and T_{DM}^{2} model ages of 2.7–2.1 Ga and 2.5–1.95 Ga, respectively. Geochemically, the Montezuma granitoids are weakly peraluminous to metaluminous magnesian granitoids, enriched in LILES and LREE, with high to moderate Mg# and depleted in some of the HFSE. Their lithochemical signature, added to the juvenile signature of both inherited and crystallized zircons, allowed its classification as a shoshonitic high Ba-Sr granitoid related to a late- to post-collisional lithosphere delamination followed by asthenospheric upwelling. In this scenario, the partial melting of the lithospheric mantle interacted with the roots of an accreted juvenile intra-oceanic arc, being these hybrid magma interpreted as the source of the Montezuma granitoids. The Córrego Tinguí Complex host rocks are akin to a syn- to late-collisional volcanic arc granitoids originated from the partial melting of ancient crustal rocks. The results presented in this study have revealed the

occurrence of juvenile rocks, probably related to an island arc environment, that are exotic in relation to the Paleo- to Neoarchean crust from the São Francisco paleocontinent's core.

Keywords: Zircon U-Pb-Hf; Titanite U-Pb; High Ba-Sr; Late- to post-collisional; São Francisco paleocontinent.

1. Introduction

Understanding Paleoproterozoic magmatic events has global significance as it informs the evolution of palaeocontinents and represents the recycling of the first continental crust formed during the Archean (e.g., Silva et al., 2002; Heilbron et al., 2010; Zhao et al., 2011; Cioffi et al., 2016; Wang et al., 2016; Patersson et al., 2018). In central Brazil, the São Francisco craton and associated marginal orogens registers several important Archean–Paleoproterozoic tectono-magmatic events playing an important role in the formation of the South American continental crust. (e.g., Barbosa and Sabaté, 2004; Heilbron et al., 2010; Cioffi et al., 2016; Cruz et al., 2016; Moreira et al., 2018).

Despite most of the continental crust formation being linked to the end of arc and collisional stages of magmatism (Hawkesworth et al., 2009), post-collisional magmas with dual mantle and crustal geochemistry also represent an important contribution to crustal growth processes (Couzinie et al., 2016).

Events of granitoid generation associated with a late to post-collisional tectonic settings are commonly related to a hybrid environment, with diferent proportions of interaction between mantle and crustal derived magmas (e.g. Bonin, 2004; Moyen et al., 2017). Consequently, some late- to post-collisional granitoids, classified as shoshonitic or high Ba-Sr granitois, have a dual mantle-crust chemical signature whose petrogenetic process are linked to the partial melting of a subduction related matassomatized mantle, with latter crustal assimilation and contamination (Bonin, 2004; Fowler et al., 2008; Goswami and Bhattacharyya, 2014; Clemens et al., 2017; Moyen et al., 2017).

The São Francisco Craton consists of a stable crustal segment not affected by the Neoproterozoic collisional and accretionary processes related to the Gondwana supercontinent construction (Almeida, 1977; Alkmim et al., 1993). As a result, several Neoproterozoic orogenic belts partly reworked its margins, being the Araçuaí orogen developed at its eastern edge (Fig. 1; Almeida, 1977; Alkmim et al., 2006). The São Francisco paleocontinent represents the Archean nuclei and Paleoproterozoic magmatic arcs amalgamated during the early Orosirian that integrate the basement of both the São Francisco craton and its marginal orogens (Noce et al., 2007; Heilbron et al., 2010; Degler et al., 2018). The so-called Rhyacian–Orosirian orogeny is marked by the production of enormous volumes of granitoids between ca. 2.35 Ga and 2.08 Ga, which were variably deformed mainly during collisional processes (Silva et al., 2002; Noce et al., 2007; Heilbron et al., 2010; Cruz et al., 2016; Silva et al., 2016), followed by extensive ca. 2.08–1.85 Ga late- to post-collisional magmatism (Santos Pinto et al., 1998; Barbosa et al., 2012; Cruz et al., 2016).

Despite recent work on the granitoid rocks that integrate the deformed segments from the São Francisco paleocontinent exposed within the Araçuaí orogen basement (e.g., Silva et al., 2002, Noce et al., 2007; Heilbron et al., 2010; Cruz et al., 2016; Silva et al., 2016; Degler et al., 2018), there are many questions still to be answered. This paper, based on new petrographic, lithogeochemical, geochronological (U-Pb in zircon and titanite) and isotopic (Hf in zircon) data from the Montezuma granitoids and its host rock, the Córrego do Tingui Complex (Knauer et al., 2007, 2015), presents the record of a high Ba-Sr juvenile magmatism at ca. 2.03 Ga constituting a new element added to the crustal growth of the São Francisco paleocontinent.

2. Geological Setting

The São Francisco paleocontinent is composed by several Archean nuclei, including the Quadrilátero Ferrífero, Gavião, Serrinha, Jequié, Guanhães and Itacambira-Monte Azul, being commonly represented by a sodic association of tonalite-trondhjemite and granodiorite complexes (TTG) and associated greenstone belts, and potassic rich granitoids (e.g. Barbosa and Sabaté, 2002; Noce et al., 2007; Romano et al., 2013;

Farina et al., 2015; Silva et al., 2016; Fig. 1B). Throughout the Paleoproterozoic, these blocks were accreted through collisional processes that resulted in the building of several orogenic belts with associated cordilleran and juvenile magmatic arcs, including the Itabuna-Salvador-Curaçá, Mineiro, Mantiqueira, Juiz de Fora and the Western Bahia, whose ages vary from Siderian to Orosirian (ca. 2.5–1.9 Ga; Barbosa and Sabaté, 2002, 2004; Noce et al., 2007; Heilbron et al., 2010; Teixeira et al., 2015; Cruz et al., 2016; Degler et al., 2018; Moreira et al., 2018; Fig. 1B). These Rhyacian to Orosirian collisional processes were responsible for the construction and consolidation of the São Francisco paleocontinent.

In addition, rifting events occurred after the assemblage of the São Francisco paleocontinent, giving rise to intra-plate anorogenic magmatism (ca. 1.75 Borrachudos and São Timóteo granitoids; Lobato, 1985; Dussin, 1994; Fernandes et al., 1994; Silva et al., 1995; Chemale et al.,1997; Silva et al., 2002; Lobato et al., 2015; Magalhães et al., 2018) and deposition of the cover units from the Espinhaço and Macaúbas supergroups (Danderfer and Dardenne, 2002; Danderfer et al., 2009, 2015; Costa and Danderfer, 2017) (Figs. 1–3). At the end of the Neoproterozoic, parts of the Archean-Paleoproterozoic rocks were reworked within the Araçuaí orogen during the Brasilian/Pan-African orogeny (Almeida, 1977; Pedrosa-Soares et al., 2001; Alkmim et al., 2006). Thus, the sector investigated here represents the extension of the São Francisco paleocontinent inside the Araçuaí orogen (Fig. 1).

At the northeastern portion of the São Francisco paleocontinent, here it is highlighted the events recorded in the Gavião and Itacambira-Monte Azul nuclei. The first one consists of Archaen gneissic-migmatitic TTG terranes, meta-volcanosedimentary sequences and potassic granitoids intruded by Paleoproterozoic granitoids, represented by twenty-nine intrusive massifs that vary in shape, size and lithogeochemical characteristics with crystallization ages from ca. 2.38 Ga to 1.85 Ga (Cruz et al., 2016 and references therein). Recently, Cruz et al. (2016) separated these granitoids into pre- to syn-collisional (ca. 2.35–2.06 Ga) and late- to post-collisional (ca. 2.05–1.90 Ga) groups based on their geochronological and lithogechemical signatures, and deformation characteristics. This Paleoproterozoic magmatism, as proposed by these authors, was related to the development of a cordilleran continental arc, the Western Bahia Magmatic Arc (WBMA, Fig. 2), in response to the collision between the Gavião and Jequié nuclei from ca. 2.3 Ga.

The Itacambira-Monte Azul nucleus can be understood as the southward continuation of the western Gavião nucleus overprinted by the Neoproterozoic Araçuaí orogeny and is also represented by Archean gneissic-migmatitic TTGs and high-k calc-alkaline granitoids (Silva et al., 2016; Bersan et al., 2018a; Figs. 1, 2). These rocks are associated with the Riacho dos Machados meta-volcanossedimentary sequence of unknown age, as well as the Paleoproterozoic granitoids of the Paciência and Catolé suites whose evolution is connected to the WBMA post-collisional stages (Silva et al., 2016; Bersan et al, 2018b; Sena et al., 2018; Figs. 1, 2).

The gneisses from Córrego Tinguí Complex area, host of the Montezuma granitoids, are located in the southern region of the Gavião nuclei, where it is exposed as a basement window (Silva et al., 2016), and is bounded by Archean TTG gneisses and Tonian supracrustal rocks of the Macaúbas Supergourp (Costa and Danderfer, 2017). It outcrops in a N–S trending structural high (Peixoto, 2017) and is ca. 15 km in width and ca. 60 km in length encompassing an area of ca. 350 km^2 (Figs. 2, 3).

2.1. Previous studies on the Córrego Tinguí Complex and Montezuma granitoids area

Knauer et al. (2007) first described the Corrego Tingui Complex as an association of equigranular to porphyritic granitoid rocks and migmatized banded gneisses, locally affected by varying intensities of Neoproterozoic tectonic deformation. The Córrego Tinguí Complex was earlier considered to be Archean (Knauer et al., 2007), however recent U–Pb zircon ages obtained by Silva et al. (2016) from banded biotite gneiss with "in situ" pockets of anatetic leucosome constrained its crystallization age at 2.14 Ga (Fig. 3). Based on their litogeochemical (data not available) and isotopic signatures (ε_{Nd} of –6.85 and T_{DM} of 3.31 Ga), Silva et al. (2016) classified these rocks as a syn-collisional granitoid with significant involvement of a Paleoarchean crustal source.

As proposed by Knauer et al. (2015), the Córrego Tingui banded gneisses are intruded by granitoids that were affected by different degrees of tectonic deformation, sorting from slightly foliated to mylonitic granitoids. In the scope of this work, these deformed granitoids were named Montezuma granitoids, due to its proximity to the Montezuma town (Fig. 3). However, as also stated by Knauer et al. (2015), the outcrops are rare and poorly preserved which preclude the identification of field relation between them. In this work, we use the chemical signature (high K_2O and Ba-Sr) and the occurrence of accessory titanite or muscovite to distinguish and classify the rocks as belonging to the Córrego Tingui Complex (low Ba-Sr and lower in K_2O, absence of titanite and presence of muscovite) and the Montezuma granitoids (high Ba-Sr, high K_2O, titanite occur as accessory phase). During field investigations, neither xenoliths nor mafic microgranular enclaves (MMEs) were observed within the Montezuma granitoids.

3. Analytical methods

New twelve lithochemical analyses were obtained from the granitoids that compose the Córrego Tingui Complex and the Montezuma granitoids. Among these, four (T7B, VM-82, T2B and T1A) were chosen for EPMA mineral chemistry analyses and two were selected for zircon U-Pb analysis (VM-82 and T1C). However, zircons from sample T1A are metamitic and the results are highly discordant, showing no reliable age (see the results in the Supplementary files). LA-ICP-MS titanite U-Pb dating was performed in the same VM-82 sample dated by zircon U-Pb geochronology. In situ zircon MC-ICP-MS Hf isotopic analyses were performed for all dated zircon crystals from sample VM-82. For details about the procedures, used techniques and equipments, detection limits and standards applied for chemical and geochronological analyses, please refers to supplementary material (Supplementary file Methods)

4. Results

4. 1. Sampling, petrography and mineral chemistry

The main outcrops are scattered and sparse. The field relationships among the different geological stations are therefore assumed. In this study we described and sampled different outcrops of the high Ba-Sr Montezuma granitoids (T2A, T2B, T2C, T3A, T3B, T5, T7A, T7B and VM82) and the Córrego Tinguí Complex granitoids (T1A, T1B, T1C). Fig. 3 shows the locations of 12 samples collected, including the sample used for U-Pb dating and Hf isotopic analysis (VM82).

The Córrego Tinguí Complex rocks (Fig. 4A–C) are medium to coarse-grained gneissified granodiorites to monzogranites, that have main mineralogy consisting of plagioclase (38%–40%), quartz (30%–33%) and alkali-feldspars (18%–20%) with minor biotite (~8%) and white-mica (2%–4%) (Fig. 4B, C). Zircon, apatite and opaque minerals are the common accessory phases. Quartz is anhedral, with sizes varying from 2 mm to 5 mm and show undulose extinction in some sections. Plagioclase (X_{An}: 4.30%–11.98%; X_{Ab}: 87.39%–95.26%) is medium to coarse-grained anhedral to subeuhedral crystals with composition varying from oligoclase to albite (Figs. 4B, C, 5A). They can have polysynthetic twinning (Fig. 4B) and are cloudy in some thin-sections due to their breakdown into sericite (Fig. 4C). The alkali-feldspars are dominantly microcline, and its orthoclase component (X_{Or}) ranges from 90.23% to 96.98% (Fig. 5A). They occur either as smaller or larger (up to 1 cm) crystals in which inclusions of plagioclase and biotite may occur (Fig. 4B). Biotite is the only mafic mineral and occurs as small to medium euhedral and subeuhedral blades within the interstices of quartz and feldspars crystals (Fig. 4B, C). The biotite from Corrego Tinguí granitoids plot in the field of ferro-biotite and are characterized by low TiO_2 contents (average of 2.23 wt.%) and medium MgO (average of 8.83 wt.%) with average Mg/(Fe^T + Mg) ratio of 0.44 (Fig. 5B–E; Supplementary Table 1). White mica is commonly described as sericite, being related to the weathering and breakdown of plagioclase crystals. However, it is also observed as euhedral to subhedral crystals associated with biotite or plagioclase (Fig. 4B, C; sample T1A). According to the division established by Miller et al. (1981) most of the analyzed white-mica from sample T1A falls in the field of secondary mica. However, some of them plot within the transition field of secondary and primary micas, as show in Fig. 5F. The accessory minerals are euhedral to subhedral and occur associated with biotite or plagioclase.

The Montezuma granitoids are equigranular to porphyritic biotite monzogranites with minor granodiorite and quartz-monzonite. These rocks are highly to slightly foliated (Fig. 4D–N), with some protomylonitc to mylonitic members (Fig. 4D–F). Its main mineralogy consists of plagioclase (30%–40%), alkali-feldspars (20%–50%), quartz (10%–30%), biotite (5%–20%), with secondary calcite, white-mica and chlorite reaching values up to 5%. Zircon, apatite, epidote, titanite and opaque minerals are the common accessory phases, while allanite was observed in few of the analysed thin-sections (Fig. 4E–O). Quartz occurs as small anhedral crystals with undulose extinction intimately associated with the feldspar-biotite groundmass (Fig. 4H, K, O). For the

Montezuma granitoids, feldspar mineral chemical analyses were done only for the dated VM-82 sample. Biotite analyses were made from three samples with distinct whole rock MgO content: T7A (less differentiated with MgO~3.2 wt.%), VM-82 (MgO~1.8 wt.%) and T2B (MgO ~1 wt.%). Plagioclase from sample VM-82 is essentially oligoclase in composition (X_{An}: 15.85%–20.46%; X_{Ab}: 78.78%–82.92%) and occurs as fine to medium grained anhedral to subhedral grains that show polysynthetic twinning (Figs. 4K, 5A). Alkali-feldspars (X_{Or} = 89.04%–93.62%; X_{Ab} = 6.37%–10.44%) are subhedral, medium to coarse grained, and dominantly classified as microcline with minor perthite, which may contain inclusions of plagioclase and biotite (Fig. 4H, K, L , O). The concentration of BaO and SrO in plagioclase (average BaO and SrO of 0.028% and 0.088%, respectively) and alkali-feldspar (average BaO and SrO of 0.63% and 0.090%, respectively) crystals from sample VM-82 are higher than those obtained for the Córrego Tinguí granodiorites (plagioclase average: BaO = 0.009%, Sr = 0.000%; alkali-feldspar average: BaO = 0.414%; SrO = 0.006%; Supplementary Table 1). Biotite is again the only mafic mineral phase and in deformed granitoids defines the protomylonitic to mylonitic foliation. Biotites from the less differentiated sample T7A (Fig. 4F) have higher MgO (average of 12.39 wt.%), lower FeO (average of 15.53 wt.%), and therefore higher Mg# (average 0.59), than the biotites from samples VM-82 (average MgO, FeO and Mg# are respectively 9.44 wt.%, 20.44 wt.% and 0.45) and T2B (average MgO, FeO and Mg# are respectively 7.72 wt.%, 21.27 wt.% and 0.39). These biotites are classified as magnesio-biotite (sample T7A) and ferro-biotite (samples VM-82 and T2B; Figs. 4F, K, L, O, 5B, C). In the $FeO^T/(FeO^T+MgO)$ vs. MgO digram (after Zhou, 1986) they plot in between mantle-crustal mixed source and purely crustal source, whereas the biotite of the Córrego Tinguí Complex plot within the crustal source field (Fig. 5D). Moreover, the $FeO–MgO–Al_2O_3$ biotite discrimination diagram (after Abdel-Rahman, 1994) suggests a calc-alkaline magma related to subduction for the Montezuma granitoids; the Córrego Tinguí biotites plot mostly in the collisional peraluminous related magmatism field (Fig. 5E). Accessory minerals are euhedral to subhedral and commonly associated with biotite or plagioclase. Titanite commonly occurs as large euhedral crystals with similar size to the main phase minerals (quartz, feldspar and biotite), sometimes included in feldspars crystals (Fig. 4K, L, M).

4.2. Whole rock major and trace elements

The twelve major and trace element compositions obtained for the Córrego Tinguí Complex and Montezuma granitoids are listed in Table 1. Classification diagrams are presented in Fig. 6. The Montezuma granitoids plot mostly within the quartz-monzonite field in the Middlemost (1985) TAS diagram with only two more evolved samples potting in the granite field; the three analyzed samples for the Córrego Tinguí Complex plot within the granite field in this diagram (Fig. 6A). In the K_2O vs. SiO_2 diagram, the Montezuma granitoid samples plot in the shoshonitic series field, whereas the Córrego Tinguí rocks have lower concentrations of K_2O, plotting in the transition area between the medium to high-K calc-alkaline fields (Fig. 6B). The shoshonitic affinities of the Montezuma granitoids are also attested by its high Th/Yb, Ce/Yb and Ta/Yb ratios (Fig. 6C; Pearce, 1982). The samples have a weakly peraluminous to metaluminous character (Fig. 6D) with Montezuma granitoids being classified as alkali to alkali-calcic, while Córrego Tinguí Complex samples plot in the calc-alkalic field (Frost et al., 2001, Fig. 6E). All samples show magnesian affinities (Frost et al., 2001; Fig. 6F) with 100×Mg# varying from 35 to 55 for the Montezuma granitoids and 33 to 42 for the Córrego Tinguí Complex (Table 1).

The analyzed samples have intermediate to high SiO_2 contents (61.58–74.35 wt.%) and moderate Al_2O_3 concentrations (14.12–16.89 wt.%). K_2O, Na_2O and CaO contents are variable, ranging of 3.15–5.81 wt.%, 2.91–4.54 wt.% and 1.09–2.84 wt.%, respectively (Table 1, Fig. 7). Montezuma granitoids are enriched in K_2O and CaO and impoverished in Na_2O (Figs. 6B, 7). Thus, the K_2O/Na_2O ratios are higher in the Montezuma granitoids ($1.19<K_2O/Na_2O<1.68$) than in the Corrego Tinguí Complex ones ($0.69<K_2O/Na_2O<0.85$). Montezuma granitoids are enriched in $Fe_2O_3^T$ (2.51–5.14 wt.%), MgO (0.9–3.44 wt.%), TiO_2 (0.37–0.86 wt.%) and P_2O_5 (0.10–0.36 wt.%) when compared to the Córrego Tinguí Complex rocks, where the concentration of these oxides varies of 1.34–1.58 wt.%, 0.35–0.53 wt.%, 0.17–0.22 wt.% and 0.03–0.06 wt.%, respectively (Table 1; Fig. 7). The Montezuma granitoids have relatively low Rb (average of 149 ppm) and high concentrations of Ba (2357–1271 ppm), Sr (1022–374 ppm), Zr (335–275 ppm), Th (22–64 ppm), Y (23–44 ppm) and V (90–20 ppm) than Córrego Tinguí samples (Table 1; Fig. 7).

There is a tendency for all granitoids to display a fractionated chondrite-normalized REE patterns, with enrichments in light rare earth elements (LREE) and depletion in heavy rare earth elements (HREE) (Fig. 8A). Some of the analyzed Montezuma granitoids samples (T7B, VM-82 and T2B) have variable Ce anomalyes probably related to post-magmatic processes. Thus, to correct these values, we applied geometric interpolation from normalized REE values. The corrected values are indicated by asterisks in Table 2 and plotted as dashed lines in Fig. 8A. The $(La/Yb)_N$ ratios vary between 10 and 54 for the Montezuma granitoid samples. The Córrego Tinguí Complex samples are depleted in REE, having higher $(La/Yb)_N$ ratios (64–7; Table 1). Also, the Montezuma granitoids have higher ΣREE (up to 708 ppm), while the ΣREE for the Córrego Tinguí Complex samples are lower than 150 ppm. All samples record a negative Eu anomaly. However, it is noted that the less differentiated samples from the

Montezuma granitoids have higher Eu/Eu* ratios (~0.85) and only a slightly negative anomaly (Fig. 8A; Table 1).

Primitive mantle normalized incompatible trace element patterns for all samples are characterized by enrichment in large-ion lithophile elements (LILE) over the high field-strength elements (HFSE; Fig. 8B). Nb, Ta, P, and Ti troughs are a common feature (Fig. 8B). Ba troughs are observed for the more differentiated Montezuma samples and for the Córrego Tinguí granitoids (Fig. 8B).

4.3. Zircon U–Pb dating

A total of ninety-four analyzes were carried out in sixty-three zircon grains extracted from sample VM82 (UTM 766990/8317190). The zircons are translucent to opaque and vary from light to dark brown. These grains are euhedral to subhedral, prismatic, have high Th/U ratios (0.12–1.68) and vary in size from 50–100 μm (wide) to 100–400 μm (long). The CL images reveal different textural types of zircons (Fig. 9A). Most of the investigated crystals are single-growth-zone grains with clear oscillatory zoning or oscillatory-zoned zircons with an inherited core, typical of igneous origin. Sometimes, zircon grains are either euhedral with no obvious zoning or blurred in CL. Complex textures characterized by convoluted zones and bright irregular domains were also observed in some zircons. All the U-Pb results are presented in Supplementary Table 2.

The reported dates show a wide temporal variation, spreading along the Concordia between Rhyacian to Statherian ages. The zircons have $^{207}Pb/^{206}Pb$ dates ranging between 2359 ± 27 Ma and 1759 ± 20 Ma and comprise at least three distinct clustered populations with weighted mean $^{207}Pb/^{206}Pb$ ages of 2123.3 ± 9.8 Ma (upper intercept age at 2128 ± 11 Ma), 1972.2 ± 9.1 Ma and 1823 ± 15 Ma (Fig. 9A, B). In general, the dates between ca. 2.24 Ga and 1.95 Ga were obtained in zircons with oscillatory zoning pattern, although some zircons with convolute zoning and metamict texture also yield these ages. For the $^{207}Pb/^{206}Pb$ ages below ca. 1.9 Ga, the zircon grains are structureless and blurred with lots of fractures and, sometimes, are related to inverse age zoning (i.e., younger cores than rims). Therefore, most of the young ages do not reflect the primary magmatic age but represent degrees of incomplete or complete resetting of older zircon grains.

4.4. Titanite U–Pb dating and Zr-in-titanite temperatures

Backscatter electron analysis of titanite grains reveals a majority of homogenous grains; sector zoning was only observed in a few crystals (Fig. 9C). Titanite grains from sample VM-82 are euhedral to sub angular and brownish in colour. Twenty-one grains were analyzed and fifteen yielded a concordia age of 2036 ± 8.7 Ma (after ^{204}Pb correction based on the weighted mean $^{206}Pb/^{238}U$ age of 2051 ± 13 Ma obtained from the uncorrected data; Fig. 9C). Three analyses are slightly discordant, with two of them defining a discordia that intercepts the concordia at 1789 ± 100 Ma (Fig. 9B).

The Zr-in-titanite temperatures were calculated using the method of Hayden et al. (2008). Although zircon and quartz are commonly observed to coexist with titanite in the analyzed samples, rutile does not coexist with titanite. Thus, the activation energy of TiO_2 (αTiO_2) is lower than 1. Given the absence of P–T–t–x modelling for the Montezuma granitoids, we considered $\alpha TiO_2 = 0.5$ and pressure estimation of 1.0 GPa for all data. The obtained temperatures vary from 712 °C to 766 °C (average of 740 °C) for the 2036 Ma concordant titanite grains; for the discordant titanite on the ca. 1.8 Ga discordia line the temperatures are 703 °C and 492 °C.

4.5. Zircon Hf isotopes

Almost all the zircon domains that have the most concordant U-Pb ages were also measured for their Hf isotope compositions and the results are listed in Supplementary Table 4 (the calculation formula and the relevant constant used in calculations are presented in the foot note of this table). The $\varepsilon_{Hf}(t)$ values were calculated using the zircon $^{207}Pb/^{206}Pb$ ages. A summary of the Hf isotope results are show in Table 2.

The $^{176}Hf/^{177}Hf_{(t)}$ ratios for sample VM82 show a wide range from 0.281325 to 0.281785 (Fig. 10A). For the oldest zircons, showing dates between ca. 2.15 Ga and 2.05 Ga, the $^{176}Hf/^{177}Hf_{(t)}$ varies from 0.281325 to 0.281669 (Fig. 10A and Supplementary Table 4). The $\varepsilon_{Hf}(t)$ for this group of ages are dominantly positive, varying from 0 to +8.87, with only one sample giving a negative $\varepsilon_{Hf}(t)$ value ($\varepsilon_{Hf}(t)$ = –4.11; Fig. 10B and Supplementary Table 4). As observed for the oldest zircons, a broad variation of the $^{176}Hf/^{177}Hf_{(t)}$, between 0.281443 and 0.281724 (Fig. 10A and Supplementary Table 4), is also typical for the ca. 2.04–1.9 Ga zircons; positive values of $\varepsilon_{Hf}(t)$ (+1.14 to +8.17) are also predominant, with four spots having negative$\varepsilon_{Hf}(t)$ values (–0.12 to –3.06; Fig. 10B and Supplementary Table 4). For the youngest zircons, with dates between ca. 1.86 Ga and 1.76 Ga, the $^{176}Hf/^{177}Hf_{(t)}$ is slightly higher and has a narrow range between 0.281638 and 0.281785, with $\varepsilon_{Hf}(t)$ varying from +0.45 to +5.48; Fig. 10 and Supplementary Table 4).

5. Discussion

5.1 - Assessment on the degree of weathering and element mobility

The presence of secondary chlorite, sericite, carbonate and epidote in the granitoid samples may indicate some degree of post-magmatic alteration or weathering. As show in chondrite-normalized REE diagram (Fig. 8A), Ce anomalies are also described for some of the analyzed samples, and may also be an indication of post-magmatic supergene processes (Cotton et al., 1993). To verify the degree of weathering of the Montezuma and Córrego Tinguí Complex granitoid rocks, we use the chemical index of alteration (CIA; molar [Al_2O_3/(Al_2O_3+CaO*+Na_2O+K_2O)]; Nesbitt and Young, 1982) and the MFW diagram proposed by Ohta and Arai (2007). The CIA values vary between 49 and 53 (Table 1) and are within the range of fresh granitoids suggested by Nesbitt and Young (1982). The MFW diagram also indicates that these rocks experienced low degrees of weathering (considering a cut-off value of W = 30%), since their position close to, or overlapping with, the igneous trend in the MFW diagram of Ohta and Arai (2007), suggests limited alteration and/or LILE (Large Ion Lithophile Elements) mobility (Supplementary Fig. 1).

5.2. Age and isotopic constraints of the Montezuma granitoids

Three main zircon age group populations between Rhyacian to Statherian where obtained for Montezuma granitoid sample VM-82 (Fig. 9). Group I comprise zircon grains with clearly igneous oscillatory zoning and ages ranging from 2.15 Ga to 2.05 Ga with a mean $^{207}Pb/^{206}Pb$ age of 2.12 Ga. Most zircons from Group II are also characterized by igneous oscillatory zoning and have crystallization ages between 2.04 Ga and 1.9 Ga with weighted mean $^{207}Pb/^{206}Pb$ age of 1.97 Ga. Group III comprises the youngest group of zircons, averaging 1.82 Ga. These zircons are structureless and metamictization is commonplace. Aditionaly, some of the grains have reverse core and rim ages, similar to those presented by Gerdes and Zeh (2009) and interpreted as fluid controlled zircon alteration.

Due to the spread of U-Pb ages in the Concordia diagram, the $^{176}Hf/^{177}Hf_{(t)}$ ratios were used to investigate coupling or decoupling between the U-Pb and Lu-Hf systems, i.e, if this range of U-Pb ages are related to multiple Pb-loss events (Gerdes and Zeh, 2009). As show in figure 10A, the three discrete groups of zircons have a distribution of $^{176}Hf/^{177}Hf_{(t)}$ ratios, although overlap between the groups exists, that is not expected for younger ages related to Pb-loss. Also, if the younger age defined by the Group II zircons were related to the process of lead-loss from the ca. 2.12 Ga Group I zircons, it would be expected a decrease in the Pb content from the older to the younger ages. However, as shown in Supplementary Fig. 2, the counts (CPS) of both ^{206}Pb and ^{207}Pb are similar or even higher for the younger group of zircon. Thus, it is unlike that dates between 2.04 Ga and 1.9 Ga obtained for Group II zircons are related to some lead-loss that affected the ca. 2.12 Ga Group I zircons.

Reconciling the crystallization age of this rock with three sub to concordant distinct groups of ages is not a straightforward task. On the other hand, titanite is potentially a good candidate to clarify this issue. Firstly, the titanite from sample VM-82 seems to be igneous, being euhedral and texturally in equilibrium with the main mineralogical assemblage (quartz, feldspars and biotite; Fig. 4K–M). Second, the large size of the titanites (Fig. 4L, M), the absence of metamorphic reaction texture in thin sections with biotite or Fe-Ti oxides, and the presence of zircon inclusions (bright response in BSE image; Fig. 9C), plausibly suggests an igneous origin for such crystals. The large size of some titanites is consistent with then avoiding Pb-loss after interaction with fluids that altered the zircons at ca. 1.8 Ga. Moreover, two discordant titanites yield an intercept age similar to the youngest group of zircons (Fig. 9B). Also, there are no corroded borders or other textures in the titanite crystals indicative of an inherited origin for these grains. Thus, among such a complex group of ages for a single rock, the authors are inclined to suggest a crystallization age at approximately 2.03 Ga for this granitoid, given the Concordia age provided by titanite after common lead correction and the oldest zircon ages of Group II (Fig. 9A). Therefore, we interpret that the older group of zircons represent inherited contributions assimilated by the magma, and the younger group is related to later hydrothermal metasomatic alteration. Also, the main metamorphic event that affected the Montezuma granitoids are Neoproterozoic in age, since its foliations are subparallel to the Neoproterozoic tectonic fabric described in the surrounding Proterozoic supracrustal sequences. Thus, if these titanites were related to the metamorphic event that causes its deformation, we should expect ages of ca. 600-500 Ma.

The inherited zircon grains from group I reflect an important contribution and/or incorporation of a heterogeneous and dominantly juvenile Paleoproterozoic ancient crust for the Montezuma granitoids magma (Fig. 10B). Combined with the juvenile Hf signature of most of the Group I zircons, the lack of inherited Archean zircons and average T_{DM} ages at 2.27 Ga within the Montezuma VM-82 sample is a contrasting feature, since its surrounding Paleoproterozoic granitoids of the WBMA have a considerable Archean contribution indicated by the presence of inherited grains and whole-rock Sm-Nd signatures (Figs. 2, 3; Cruz et al., 2016; Silva et al., 2016 and references there in). Therefore, it is unlikely that these grains were captured from the WBMA continental crust. Possible sources for these inherited zircons are the ca. 2.17 to 2.10 juvenile granitoids from the Mineiro belt (eg. Barbosa et al., 2015; Moreira et al., 2018) or the ca. 2.15 Ga and 2.08 Ga Juiz de Fora/Pocrane complexes rocks (Degler et al., 2018), southern São Francisco paleocontinent (Fig. 1), which have the same range of ages and similar Hf isotopic signature (Fig. 10). Despite that, the heterogeneous (ε_{Hf} of +8.14 to –3.06) but dominantly juvenile signature of group II zircons (Fig. 12B), interpreted as the crystallization age of the Montezuma granitoids, points to a mixed source with some degree of mantle input, since their $\varepsilon_{Hf}(t)$ can be as high as the inherited zircons. If its source was only related to melting of a relatively homogeneous ancient crust, it would be expected to yield lower and less variable $\varepsilon_{Hf}(t)$ values, and not within the same range as observed. The crystallization age estimated for the Montezuma granitoids coincides with the timing of major late- to post-collisional magmatism and orogenic collapse that was followed by a period of slow cooling and final stabilization of the São Francisco paleocontinent continental mass at ca. 1.9 Ga (Heilbron et al., 2010; Cruz et al., 2016; Silva et al., 2016; Aguilar et al., 2017).

In the São Francisco paleocontinent, similar ages to the group III zircons are related to the Espinhaço rift related Statherian (ca. 1.75 Ga) A-type granitoids (Borrachudos Suite and Lagoa Real Complex; Dussin, 1994; Fernandes et al., 1994; Silva et al., 1995; Chemale et al.,1997; Dussin et al., 1997; Silva et al. 2002; Lobato et al., 2015; Figs. 1, 2), as well as some mafic to acid volcanic rocks associated with the Espinhaço rifting basal units (Danderfer et al, 2009; Danderfer et al., 2015; Costa et al., 2017; Moreira, 2017; Fig. 3). This rifting event affected almost the entire eastern part of the São Francisco paleocontinent and disturbed the isotopic record of Group III zircons, causing isotopic re-setting and inverse age zoning. The imprints of this rifting event on zircons from Paleoproterozoic granitoids was also noticed by Degler et al. (2018) for juvenile rocks of the Juiz de Fora/Pocrane complexes.

5.3. Classification of the Montezuma granitoids

Granitoid rocks are commonly classified according to their affinity to I, S, M and A-types. These classifications are mainly based on the mineralogical and geochemical characteristics of the granitoid rock, and may further be linked to the nature of source rocks or to the tectonic setting (Pitcher, 1997).

The lithochemical composition of the Montezuma granitoids show that these rocks are slightly peraluminous to metaluminous and characterized by moderate to high concentrations of some major oxides (MgO, CaO, K_2O, TiO_2 and P_2O_5), with relatively high Mg# (35–55), for values of SiO_2 ranging of ca. 61–70 wt.%. Moreover, they are enriched in LILEs (Ba and Sr that reaches concentrations higher than 1000 ppm), as well as in REE and in some of the transition elements (Zr, Y and V). Although the Montezuma granitoids share some similar features with A-type granitoids, such as the

K_2O, Zr, Nb and Ce concentrations, their low SiO_2 and 10,000×Ga/Al ratios (<2.6), as well as their magnesian affinity, contrasts with the typical A-type signature (Figs. 6F, 11A, B; Whalen et al., 1987; Frost et al., 2001).

Regarded as a distinct group of granitic rocks, Tarney and Jones (1994) proposed the high Ba-Sr granitoid group, which is characterized by unusual trace element contents, as high K/Rb, Ba (>500 ppm), Sr (>300 ppm; Ba+Sr >1500 ppm) and light REEs; relatively low Rb/Sr ratios, Nb, Ta and heavy REEs. As previously described, the chemical signature obtained for the Montezuma granitoids, such as its high Ba, Sr and LREE contents along with low abundance of HREE and its $(La/Yb)_N$ (18.07–53.76) and Sr/Y (22–35) ratios, are similar to the high Ba-Sr granitoids (Tarney and Jones, 1994; Fowler et al., 2008; Fig. 11C). The Montezuma granitoids have a shoshonitic affinity (Fig. 6B, C) and share characteristics (e.g. their relatively high K_2O/Na_2O ratios and high P_2O_5, ΣREE and LREE/HREE ratios, Ba, Sr, and Zr) of late- to post-collisional shoshonitic type granitoids (Jiang et al., 2002; Goswami and Bhattacharyya, 2014; Clemens et al., 2017). Thus, the Montezuma granitoids can be classified as high Ba-Sr shoshonitic granitoid. Some chemical characteristics of the Montezuma granitoids resemble the signature of Archean granitoids from the sanukitoid series (Laurent et al. 2014), a characteristic also presented by other shoshonitic granitoids (Fig. 11E; Goswami and Bhattacharyya, 2014; Clemens et al., 2017). However, despite the relatively high Mg#, the high K_2O and K_2O/Na_2O ratios, togheter with the lack of Ni and Cr analyses in this study, make it difficult to classify these rocks as typical sanukitoid-like granitoids.

High Ba–Sr and shoshonitic granitoids can be formed by similar processes (e.g. Tarney and Jones, 1994; Fowler et al., 2008; Goswami and Bhattacharyya, 2014; Clemens et al., 2017). According to Tarney and Jones (1994), the generation of high Ba–Sr granitoids can be related to partial melting of subducted ocean islands or ocean plateaus; partial melting of underplated mafic rocks; or partial melting of lithospheric mantle that had been metasomatized by asthenosphere-derived carbonatitic melts. Some authors attributed their origin to the partial melting of the mafic lower crust (with residual garnet) (Ye et al., 2008; Choi et al., 2009) or to AFC products of mantle-derived appinitic magmas (Fowler et al., 2001, 2008). For the shoshonitic type granitoids, Jiang et al. (2002) proposed two different mechanisms of generation: involvement of subducted oceanic crust sediments into the mantle source; or partial melting of subducted oceanic crust sediments or metasediments of the thickened continental lower crust in the process of late-orogenic slab break-off or lithospheric thinning. According to Jiang et al. (2006), Jiang et al. (2012), Goswami and Bhattacharyya (2014) and Clemens et al. (2017), partial melting of an enriched lithospheric mantle, metasomatized by slab-derived fluids or hybridized by continental slab-derived melts could explain the signature of some shoshonitic type granitoids. Partial melting of a lower crustal incompatible-element enriched amphibolite source is also proposed for the generation of shoshonitic granitoids (Bitencourt and Nardi, 2004). So, although the origin of both high Ba–Sr and shoshonitic granitoids are not well constrained, and there is a lot of discussion about their genesis, they are believed to be related to a late to post-collisional tectonic setting.

The São Francisco paleocontinent was in a late- to post-collisional setting during the early Orosirian, precluding a source related to partial melting of subducted ocean islands or plateaus. Also, the Montezuma granitoids have low Sr/Y (Fig. 11D), which also precludes any relation to adakite-like granitoids generated by the partial melting of thickened lower crust.

The lack of field evidence of the interaction between basic and acid granitic magmas (e.g. evidence of magma mingling and mafic enclaves) within the Montezuma granitoids coupled with the abundance of inherited zircon grains may suggest granitic melts extracted from juvenile crustal sources only. However, the Mg# values of the Montezuma granitoids reaches values of 55, which are relatively higher than those expected for a mafic lower crustal source (Rapp and Watson, 1995; Rapp et al., 1999).

The high Mg# coupled with a juvenile εHf isotopic signature indicate that the primary magma of the Montezuma granitoids are at least partly derived from, or interacted with, a mantle source. In addition, a mantle-crust mixed magmatic source is also indicated by its biotite compositions (Fig. 5D), which are consistent with the interpretation of a mantle-crust mixed origin. In this case, the enrichment in incompatible elements may indicate either some crustal contamination during or after the magma emplacement or that its source was already enriched, metasomatized by fluids or melts during previous subduction events. The process of crustal contamination does not seem to be a controlling factor, since the concentration in incompatible elements of the less diferentiated Montezuma granitoids are higher than its host rocks. Thus, it is more reasonable to interpret that its source was already enriched in those elements.

The alkali-calcic to alkalic, high-K to shoshonitic affinities of the Montezuma granitoids preclude that they are classical arc magmas. The main geochemical features of the Montezuma granitoids are similar to late- to post-collisional suites affected by prior subduction events with later metasomatism of the lithospheric mantle. The late- to post-collisional nature of these rocks is supported by the tectonic discrimination diagram of Pearce et al. (1984) (Fig. 11F).

The ratios between fluid/melt-mobile and fluid/melt-immobile trace elements can be used to evaluate the importance of subduction fluids (enrichment in Ba, Sr and Nb, for example) and/or sediment melts (enrichment in Th and LREE) in the metasomatism of its source. The low Th/Nb ratios of the Montezuma granitoids point to a contribution from slab-derived fluids (Fig. 12A). However, Nebel et al. (2007) proposed that fluid-dominated arc environments have low Th/Yb ratios (commonly <1), whereas arc settings dominated by subducted sediments have high Th/Yb ratios. The Montezuma granitoids have high Th/Yb ratios (8.34–11.59), indicative of a significant contribution from sediments in its metasomatized source (Fig. 12B). The role of sediment melt in its source is also highlighted by the relatively high La/Sm ratio and low Ba/Th ratio (Labanieh et al., 2012; Fig. 12C). In this case, due to the dominantly juvenile signature of the Montezuma granitoids, the time between source metasomatism and extraction has to be relatively short.

As discussed above, the lack of Archean inheritances, together with Hf model ages below ca. 2.5 Ga (with the exception of one zircon grain for which the its Hf model age is 2.69 Ga) and its dominantly juvenile signature strongly suggest that the source of the Montezuma granitoids were generated without contribution from the Archean continental margin of the São Francisco paleocontinent, possibly related to an intra-oceanic setting. The Hf model ages obtained for the inherited zircons are within the range to those obtained for the 2.35 Ga TTG's and 2.13 Ga sanukitoids from the Mineiro belt (Moreira et al., 2018) as well as for the 2.20–1.97 Ga intra-oceanic Juiz de Fora/Pocrane complexes (Heilbron et al., 2010 and Degler et al., 2018). However, the Montezuma rocks plot within the continental arc field in the Th/Yb vs. Nb/Yb diagram (after Condie and Kröner, 2013; Fig. 12D). Some authors argue that oceanic arcs can evolve to continental arcs when they are accreted to a continental margin (ex. Draut et al., 2009; Condie and Kröner, 2013; Cioffi et al., 2016). In this case, the accreted oceanic arc becomes thicker and starts to melt its roots, generating granitoids with a continental arc-like signature (Draut et al., 2009; Condie and Kröner, 2013; Cioffi et al., 2016). Therefore, we suggest here that the Montezuma granitoids were a delayed response to a delamination process resulting from the interaction of a subcontinental mantle wedge and the roots of an accreted island arc, possible associated with a late-orogenic slab break-off or lithospheric thinning tectonic setting that was followed by the cratonization of the São Francisco paleocontinent. Alternatively, due to the complex U-Pb zircon and titanite results, these rocks could also represent a shoshonitic association related to a Paleoproterozoic mature arc. In this case, its crystallization age would have to be represented by the ca. 2.12 Ga Group 1 zircons, being the youger Group II zircon and the titanite dates related to a younger overprinting event. However, as presented above, our U-Pb data do not favor this interpretation, although, chemically, it is also a valid hypothesis.

The more differentiated samples from the Montezuma granitoids (samples T2B, T2C and T2A) were probably derived from fractional crystallization of the less differentiated Montezuma granitoids, manly controlled by feldspar, biotite, apatite and Fe-Ti oxides fractionation (more pronounced Eu anomalies, enrichment in Rb and Ba and Sr troughs; negative correlation of major and trace elements; Figs. 7, 8). Also, its lower Mg#, relatively higher A/CNK and biotite chemical signature are more crustal like, pointing to a minor participation of the mantle and, perhaps, contribution of sediments in the evolution of these samples.

An alternative explanation for the abundant inherited zircons, the heterogeneous εHf and the relatively high concentrations in Th within the Montezuma granitoids is that these grains are linked to subducted sediments (mélanges) created by the erosion of a juvenile intra-oceanic arc that were first recycled by the slab-derived melts into the mantle wedge above the subducting slab and then extracted by the Montezuma source melt (e.g.: Jiang et al., 2012; Marschall and Schumacher, 2012; Cruz-Uribe et al., 2018).

5.4 - Classification of the Córrego Tinguí Complex granitoids

The Córrego Tinguí Complex rocks chemically correspond to a magnesian, slightly peraluminous, calc-alkaline, medium- to high-K acid–silicic series and resemble a volcanic arc-like signature (Figs. 6, 11F). Although the occurrence of a small amount of muscovite and its slightly peraluminous signature resembles S-type granites, its relatively high Na_2O and low K_2O/Na_2O ratios (0.69–0.85) and the absence of other Al-rich minerals (such as cordierite and/or garnet) are more akin to an I-type signature. These rocks plot in the hybrid granites field in the Laurent et al. (2014) ternary classification diagram, where TTG field overlaps the biotite-two-mica granites field (Figure 11E). Indeed, the Córrego Tinguí granitoids share some characteristics with Archean TTG, such as: calc-alkaline, slightly peraluminous, silica-rich signature; low contents of ferro-magnesian oxides (FeO^T + MgO + MnO + TiO_2 ~2 wt.%), Y (< 5.3 ppm), Yb (~0.3 ppm), HFSE and low K_2O/Na_2O ratios; and its fractionated REE pattern ($64 \leq (La/Yb)_N \leq 97$) and relatively high Sr/Y ratios (26–35). Although their Sr/Y ratios resembles some TTGs, the Sr concentration (140–170 ppm) is too low compared to typical TTGs (usually higher than 300 ppm; Martin et al., 2005; Laurent et al., 2014). Thus, we interpret that the Córrego Tinguí rocks may represent syn-to-late collisional volcanic arc magmatism originated from the partial melting of ancient TTG-like rocks from the Gavião nuclei. Also, its biotite composition is suggestive of collisional crustal source magma (Fig. 5D, E). It is possible that these rocks resembles to the sample dated by Silva et al. (2016) at 2140 ± 14 Ma, being in this case related to a collisional setting within the São Francisco paleocontinent. Also, its chemical signature indicates the reworking of ancient basement rocks, pointing to a similar isotopic composition to the obtained by Silva et al. (2016), in which negative ε_{Hf} value of –6.85, coupled with a depleted mantle model age of 3.31 Ga, could be related to the reworking of Archean TTG's from the Porteirinha Complex. However, for further constraints on the evolution of the Córrego Tinguí Complex granitoids new isotopic studies are required.

5.5. Implications for the Paleoproterozoic evolution of the eastern São Francisco paleocontinent

The Siderian to Orosirian accretionary to collisional tectonic evolution of the eastern São Francisco paleocontinent is well constrained in its northern and southern domains (Fig. 1; Alkmim and Teixeira, 2017; Barbosa and Barbosa, 2017; Heilbron et al., 2017; Teixeira et al., 2017). In its southern domain at least three magmatic arcs were developed and/or accreted to the former Archean São Francisco paleocontinent (Fig. 1): the ca. 2.35–2.1 Ga Minas orogeny (Mineiro belt) that is composed of a set of individual juvenile and continental arc systems, each one comprising metaigneous rocks and associated supracrustal sequences (Ávila et al., 2010, 2014; Seixas et al., 2012, 2013; Barbosa et al., 2015; Teixeira et al., 2015; Moreira et al., 2018); the ca. 2.20-2.05 Ga Mantiqueira Complex, which represents a continental magmatic arc with significant Achaean crustal inheritance (Silva et al., 2002; Noce et al., 2007; Heilbron et al., 2010); the ca. 2.20–1.95 Ga, dominantly juvenile, Juiz de Fora/Pocrane intra-oceanic arc (Heilbron et al., 2010; Novo, 2013; Degler et al., 2018). In the northern domain, which encompasses the granitoids described in this work, most of the Paleoproterozoic collisional to post-collisonal magmatic rocks resemble an active continental arc, defined by Cruz et al (2016) as the WBMA (Fig. 2), although the authors suggests the possibility of a juvenile source mixed with Archean crust at ca. 2.0 Ga. Due to its similarities to the Mantiqueira arc, Cruz et al. (2016) proposed that both the WBMA and Mantiqueira arcs, based on their isotopic signatures and Archean inheritance, represents a single continental magmatic arc developed at the eastern boundary of the São Francisco paleocontinent. On the other hand, these authors also have suggested the presence of a Rhyacian juvenile accretion episode within the WBMA, based on less negative εNd signature of some late- to post-collisional granitoids, which allowed then to bring up the possibility of a linkage with the Mineiro belt granitoids.

The results obtained in this work, added to the isotopic results of Silva et al. (2016), show that the Córrego Tinguí granitoids are akin to the WBMA and Mantiqueira arcs, representing a continental-like signature whose source is related to the reworking of ancient Archean crust. However, as an exception of previous studies developed in this area, the ca. 2.13 Ga zircon inherited ages from the Montezuma granitoids record an important event of juvenile magmatism. The data obtained here suggest that the Montezuma granitoids source was originated at distance from the Archean São Francisco paleocontinent margin, probably in an intra-oceanic setting, since no Archean inheritance was observed. As discussed above, all these features likely suggest the juvenile rocks from the Mineiro belt or Juiz de Fora/Pocrane complexes as a potential source.

Hereby, the Montezuma granitoids are interpreted as a consequence of post-collisional delamination of subducting lithosphere, inducing asthenospheric upwelling that caused partial melting and interacted with a juvenile lower crust, represented by the roots of an island arc that might be represented either by the juvenile rocks from the Mineiro belt or the Juiz de Fora/Pocrane arc Consequently, the interaction of these magmas resulted in the intermediate to acid magma of the Montezuma granitoids.

Shoshonitic granitoids of almost similar age (ca. 2.05 Ga) and similar nature (high-K, Mg#, Ba and Sr) are commom to the west of the Montezuma granitoids, within the western Gavião and Itacambira-Monte Azul nuclei (e.g., Paciencia and Guanambi suites; Fig. 2). These rocks are also related to a late- to post-collisional tectonic system associated with the partial melting of metasomatized lithospheric mantle due to delamination of subducting lithosphere (Rosa et al., 1996; Rosa, 1999; Bersan et al., 2018). However, despite the similarities between these rocks and the Montezuma granitoids, they show an evolved isotopic signature, with negative ε_{Hf} (–10.88 to –7.5; Rosa, 1999; Silva et al., 2016) and ε_{Hf} (–16.8 to –18.5). Consequently, even with a similar tectonic situation, the contrasting isotopic signature points to a complex scenario involving two different sources for the setting of these Paleoproterozoic shoshonitic high Ba-Sr granitoids. Thus, we envisage the process of double subduction zones with the same polarity as proposed by Noce et al. (2007) for the southern São Francisco paleocontinent, similar to the geodynamic model proposed by Eglinger et al. (2018) for post-collisional potassic magmatism with contrasting isotopic source within the West African craton (Guinea), for the evolution of the studied post-collisional granitoids (Fig. 13). We also consider, as already stated by Mascarenhas (1979) and Barbosa et al. (2013), that the Gavião nuclei is characterized by distinct Archean paleoplates (Guanambi-Correntina block to the west, and Gavião block to the east) that collided toghether during the early stages of the Siderian–Orosirian accretionary to collisional tectonic evolution. In the proposed model, the sources from which the Montezuma granitoid magmas have been extracted were enriched by juvenile subducted sediments (with some participation of fluids) derived from an island arc (similar to the Mineiro belt or Juiz de Fora/Pocrane complexes), whereas the Paciencia and Guanambi suite sources were enriched with participation of Archean components from a continental arc developed at eastern margin of the São Francisco paleocontinent (Fig. 13A). This accretionary to convergent context occurred between ca. 2.35 Ga and 2.08 Ga (Cruz et al., 2016; Barbosa and Barbosa, 2017; Heilbron et al., 2017). By this time, the collision between the intra-oceanic arc-like and the continental arc may have thickened the lithosphere along the margin of the São Francisco paleocontinent. The Corrego Tingui Complex granitoids would have been generated during this collisional event. From ca. 2.08 Ga to ca. 1.9 Ga, a late- to post-collisional regime started to operate, and the processes of slab break-off and lithospheric delamination triggered the partial melting of lithospheric mantle and the roots of the ancient crust to produce the potassic magmas (Fig. 13B). However, the connections and relations between the WBMA and the juvenile sector of the Montezuma granitoids deserves further study in order to better constrain the tectonic evolution of the São Francisco paleocontinent. Another question still to be answered is how this predominantly Paleoproterozoic juvenile segment may be surrounded by the Archean Gavião nuclei (Fig. 2).

6. Conclusions

Our focused study of the Montezuma granitoids and its host rocks, the Corrego Tingui Complex, situated in the northestern part of the São Francisco paleocontinent provides new, significant insights for the post-collisional magmatism in this tectonic domain. Some of the most salient conclusions of this study are as follows:

(i) The Montezuma zircon U-Pb dates spread along the Concordia from ca. 2.2 Ga to ca. 1.8 Ga and can be divided into three diferent groups: Group I zircons are interpreted as inherited and have a mean $^{207}Pb/^{206}Pb$ age of 2.12 Ga; Group II zircon ages vary from 2.04 Ga to 1.9 Ga and the oldest zircon grains from this group, with mean $^{207}Pb/^{206}Pb$ age of 2026 Ma, are interpreted as the crystallization age of the Montezuma granitoids; Group III comprises the youngest group of zircons, averaging of 1.82 Ga, and are interpreted as fluid controlled zircon alteration related to the Espinhaco rifting event that affected the eastern border of the São Francisco paleocontinent.

(ii) Titanite dates constrain the Montezuma granitoids crystallization age at 2.036 Ga.

(iii) Magmas of the Montezuma granitoids are enriched in LREEs and LILEs, depleted in HFSE, with high to moderate Mg# and dominantly positive $\varepsilon_{\mathrm{Hf}}(t)$ values without Archean zircon inheritance. These geochemical and isotopic signatures allow its classification as a hybrid post-collisional high Ba-Sr shoshonitic granitoid related to the process of subducting lithosphere delamination followed by asthenospheric upwelling that caused partial melting of the roots of an accreted juvenile intra-oceanic arc.

(iv) The Córrego Tinguí Complex is akin to syn- to late-collisional volcanic arc magmatism originated from the partial melting of ancient TTG-like crustal rocks.

(v) The Montezuma granitoids, together with other post-collisional high Ba-Sr shoshonitic rocks that occur in to the west of the study area reveal a complex scenario involving two contrasting isotopic sources for the setting of these Paleoproterozoic.granitoids.

Acknowledgements

We would like to thank the financial support provided by FAPEMIG (CRA-APQ-00125-12) and the Coordenação de Aperfeiçoamento de Pessoal de Nível Superior (CAPES), by granting a PhD scholarship to S.M. Bersan (Process No. 88881.188438/2018-01 of PDSE Program No. 47/2017). To the Microscopy and Microanalysis Laboratory (LMIc) of the Universidade Federal de Ouro Preto, a member of the Microscopy and Microanalysis Network of Minas Gerais State/Brazil/FAPEMIG, for the mineral chemistry analyses. G. Queiroga and C. Lana are Fellows of the Brazilian Research Council (CNPq) and acknowledge the support received. Our gratitude goes to Monica Heilbron and an anonymous reviewer for their helpful corrections and suggestions on the former version of this manuscript, and to Kristoffer Szilas editorial handling.

References

Abdel-Rahman, A.M., 1994. Nature of biotites from alkaline, calc-alkaline and peraluminous magmas. Journal of Petrology, 35, 525–541.

Aguilar, C., Alkmim, F.F., Lana, C., Farina, F., 2017. Paleoproterozoic assembly of the São Francisco Craton, SE Brazil: New insights from U-Pb titanite and monazite dating. Precambrian Research, 289, 95-115.

Aleinikoff, J.N., Wintsch, R.P., Tollo, R.P., Unruh, D.M., Fanning, C.M. and Schmitz, M.D., 2007. Ages and origins of rocks of the Killingworth dome, south-central Connecticut: Implications for the tectonic evolution of southern New England. American Journal of Science, 307(1), 63-118.

Alkmim, F.F., Marshak, S., Pedrosa-Soares, A.C., Peres, G.G., Cruz, S.C.P., Whittington, A., 2006. Kinematic Evolution of the Aracuaí-West Congo orogen in Brazil and Africa: Nutcracker tectonics during the Neoproterozoic assembly of Gondwana. Precambrian Research, 149:43-64. https://doi.org/10.1016/j.precamres.2006.06.007

Alkmim, F.F., Teixeira, W., 2017. The Paleoproterozoic Mineiro Belt and the Quadrilátero Ferrífero. In: Heilbron M., Cordani U.G., Alkmim F.F. (Eds.). São Francisco Craton, Eastern Brazil: Tectonic Genealogy of a Miniature Continent. Switzerland, Springer International Publishing, p. 71-94.

Almeida, F.F.M., 1977. O cráton do São Francisco. Revista Brasileira de Geociências, 23(7):349-364 (in Portuguese).

Barbosa J.S., Sabaté P. 2004. Archean and Paleoproterozoic crust of the São Francisco cráton, Bahia, Brazil: geodynamic feactures. Precambrian Research, 133(3):1-27. DOI: 10.1016/j.precamres.2004.03.001

Barbosa, J. S. F., Cruz, S. P., Souza, J. S., 2012. Terrenos Metamórficos do Embasamento. In: J. S. F. Barbosa, J. F. Mascarenhas, L. C. Corrêa-Gomes, J. M. L. Dominguez, J. S. de Souza, Geologia da Bahia: Pesquisa e atualização (v. 1, 101-199). Salvador: CPBM; UFBA (in Portuguese with English abstract).

Barbosa, J.S.F., Barbosa R.G., 2017. The Paleoproterozoic Eastern Bahia Orogenic Domain. In: Heilbron M., Cordani U.G., Alkmim F.F. (Eds.). São Francisco Craton, Eastern Brazil: Tectonic Genealogy of a Miniature Continent. Switzerland, Springer International Publishing, p. 57-69.

Barbosa, J.S.F., Sabate, P., 2002. Geological feature and the paleoproterozoic of four archean crustal segments of the São Francisco Craton, Bahia, Brazil. A syntesis. Anais da Academia Brasileira de Ciências, 2, 343-359

Barbosa, N.S., Teixeira, W., Avila, C.A., Montecinos, P.M., Bongiolo, E.M., 2015. 2.17-2.10 plutonic episodes in the Mineiro belt, São Francisco Craton, Brazil: UpPb ages, geochemical constraints and tectonics. Precambrian Research, 270: 204-225.

Bersan S.M., Danderfer F.A., Abreu F.R., Lana C. 2018a. Petrography, geochemistry and geochronology of the potassic granitoids of the Rio Itacambiruçu Supersuite: implications for the Meso- to Neoarchean evolution of the Itacambira-Monte Azul block. Brazilian Journal of Geology, 48:1-24.

Bersan S.M., Danderfer F.A., Abreu F.R., Lana. 2018b. Geoquímica e geocronologia da Suíte Paciência: implicações para o fim da evolução riaciana do Bloco Itacambira-Monte Azul. Geologia USP. Série Científica, 18:185 (in Portuguese with English abstract).

Bitencourt, M. F., Nardi, L. V. S., 2004. The role of xenoliths and flow segregation in the genesisand evolution of the Paleoproterozoic Itapema Granite, a crustally derived magma of shoshonitic affinity from southern Brazil. Lithos, 73, 1-19.

Blichert-Toft, J., Puchtel, I.S., 2010. Depleted mantle sources through time: evidence from LueHf and SmeNd isotope systematics of Archean komatiites. Earth and Planetary Science Letters, 297, 598-606.

Bouvier, A., Vervoort, J.D., Patchett, P.J., 2008. The Lu-Hf and Sm-Nd isotopic composition of CHUR: constraints from unequilibrated chondrites and implications for the bulk composition of terrestrial planets. Earth and Planetary Science Letters, 273, 48-57.

Chemale Jr., F; Quade, H., Schmus, W.R.V., 1997. Petrography, Geochemistry and Geochronology of the Borrachudo Granite, Minas Gerais, Brazil. Zentralblatt für Geologie und Paläontologie. Teil 2, Paläontologie, Stuttgart, v. 3-6, 739-750.

Chew, D.M., Petrus, J.A. and Kamber, B.S., 2014. U–Pb LA–ICPMS dating using accessory mineral standards with variable common Pb. Chemical Geology, 363, 185-199.

Clemens J.D., Buick I.S., Frey D., Lana C., Villaros A., 2017. Post-orogenic shoshonitic magmas of the Yzerfontein pluton, South Africa: the ‘smoking gun’ of mantle melting and crustal growth during Cape granite genesis?. Contributions to Mineralogy and Petrology, 172:72.

Choi, S.G., Rajesh, V.J., Seo, J., Park, J.W., Oh, C.W.,Pak, S.J., Kim, S.W., 2009. Petrology, geochronology and tectonic implications of Mesozoic high Ba–Sr granites in the Haemi area, Hongseong Belt, South Korea. Island Arc 18, 266–281.

Cioffi, C.R., Campos Neto, M.C., Möller, A., Rocha, B.C., 2016. Paleoproterozoic continental crust generation events at 2.15 and 2.08 Ga in the basement of the southern Brasília Orogen, SE Brazil. Precambrian Research, 275, 176-196.

Condie, K.C., Kröner, A., 2013. The building blocks of continental crust: evidence for a major change in the tectonic setting of continental growth at the end of the Archean. Gondwana Research, 23, 394–402.

Costa, A.F.O, Danderfer, A., 2017. Tectonics and sedimentation of the central sector of the Santo Onofre rift, north Minas Gerais, Brazil. Brazilian Journal of Geology, 47, 491-519.

Costa A.F.O. 2017. Evolução tectonoestratigráfica da porção norte do Espinhaço Central, norte de Minas Gerais. PhD Thesis, Departamento de Geologia da Universidade Federal de Ouro Preto, Ouro Preto, 228p (in Portuguese with English abstract).

Costa A.F.O., Danderfer A., Bersan S.M. 2017. Record of a Statherian rift-sag basin in the Central Espinhaço Range: Facies characterization and geochronology. Journal of South American Earth Sciences, 82:311-328.

Cotton, J., Le Dez, A., Bau, M., Caroff, M., Maury, R.C., Dulski, P., Fourcade, S., Bohn, M., Brousse, R., 1993. Origin of anomalous rare-earth element and yttrium enrichments in subareially exposed basalts: evidence from French Polynesia. Chemical Geology, 119, 115–138.

Couzinié, S., Laurent, O., Moyen, J.F., Zeh, A., Bouihol, P., Villarios, A., 2016. Post-collisional magmatism: Crustal growth not identified by zircon Hf–O isotopes. Earth and Planetary Science Letters, 456, 182-195.

Cruz, S.C.P., Barbosa, J.S.F., Barbosa, A.C., Jesus, S.S.G., Medeiros, E.L.M., Figueiredo, B.S., Leal, A.B.M., Lopes, P., Souza, J.S., 2014. Mapeamento Geologico e

Levantamentos de Recursos Minerais das Folhas Espinosa e Guanambi, escala 1:100.000. Convenio UFBA/CPRM/FAPEX, Salvador, 253p. 2 mapas.

Cruz, S.C.P., Barbosa, J.S.F., Pinto, M.S., Peucat, J.J., Paquette ,J.L., Santos de Souza, J., de Souza Martins, V., Chemale Júnior, F., Carneiro, M.A. 2016. The Siderian-Orosirian magmatism in the Archean Gavião Paleoplate, Brazil: U-Pb geochronology, geochemistry and tectonic implications. Journal of South American Earth Sciences, 69:43-79. DOI: 10.1016/j.jsames.2016.02.007

Cruz-Uribe, A.M., Marschall, H.R., Gaetani, G.A., Roux, V., 2018. Generation of alkaline magmas in subduction zones by partial melting of mélange diapirs—An experimental study. Geology, 46(4): 343-346.

D'Agrella Filho, M.S, Cordani, U.G., 2017. The paleomagnetic record of the São Francisco-Congo Craton. In: Heilbron, M., Cordani, U.G., Alkmim, F.F. (eds.). São Francisco Craton, eastern Brazil: tectonic genealogy of a miniature continent. New York, NY: Springer Berlin Heidelberg; 2017.

Dandefer, A., Lana, C.C., Nalini, H.A., Costa, A.F.O., 2015. Constraints on the Statherian evolution of the intraplate rifting in a Paleo-Mesoproterozoic paleocontinent: New stratigraphic and geochronology record from the eastern São Francisco Craton. Gondwana research, 28: 668-688.

Danderfer, A., Dardenne, M.A., 2002. Tectonoestratigrafia da bacia Espinhaço na porção centro-norte do cráton do São Francisco: registro de uma evolução poli-histórica descontínua. Revista Brasileira de Geociências, 32(4): 449-460 (in Portuguese with English abstract).

Danderfer, A., Waele, B.D., Pedreira, A.J., Nalini, H.A., 2009. New geochronological constraints on the geological evolution of Espinhaço basin within the São Francisco Craton - Brazil. Precambrian Research, 170: 116–128.

Degler, R., Pedrosa-Soares, A., Novo, T., Tedeschi, M., Silva, L.C., Dussin, I., Lana, C., 2018. Rhyacian-Orosirian isotopic records from the basement of the Aracuai-Ribeira orogenic system (SE Brazil): Links in the Congo-Sao Francisco palaeocontinent. Precambrian Research, 317: 179-195.

Draut, A.E., Clift, P.D., Amato, J.M., Blusztajn, J., Schouten, H., 2009. Arc-continent collision and the formation of continental crust: a new geochemical and isotopic record from the Ordovician Tyrone Igneous Complex, Ireland. J. Geol. Soc. London, 166, 485–500.

Drummond, M.S., Defants, M.J., 1990. A model for Trondhjemite-Tonalite-Dacite genesis and crustal growth via slab melting: Archean to modern comparisons. Journal of Geophysical Research, 95, 21503-21521.

Dussin T. M., 1994. Associations plutono-volcaniques de l'Espinhaço méridional (SE-Brésil): un exemple d'évolution de la croûte protérozoïque. Lab. Geologie Structurale, Univ. Orléans, Orléans, Tese de Doutoramento, 177 p (in Portuguese).

Dussin T.M., Dussin I.A., Noce C.M. 1997. Tectonic settig and origin of the Mesoproterozoic Borrachudos granites (MG, Brazil). In: South-American Symp. on Isotope Geology, 1, São Paulo, Anais, 1:104-106.

Eglinger, A., Thébaus, N., Zeh, A., Davis, J., Miller, J., Parra-Avila, L.A., Loucks, R., McCuaig, C., Belousova, E., 2017. New insights into the crustal growth of the Paleoproterozoic margin of the Archean Kéména-Man domain, West African craton (Guinea): Implications for gold mineral system. Precambrian Research, 292: 258-289.

Farina F., Albert C., Lana C. 2015. The Neoarchean transition between medium-and high-K granitoids: Clues from the Southern São Francisco Craton (Brazil). Precambrian Research, 266:375-394. https://doi.org/10.1016/j.precamres.2015.05.038

Fernandes, M.L.S., Marciano, V.R.P.R., Oliveira, R.C., Neves, J.M.C., Diláscio, M.V., 1994. Granitos Borrachudos: um exemplo de granitogênese anorogênica na porção central do estado de Minas Gerais. Geonomos, 2, 23-29 (in Portuguese).

Fowler, M.B., Henney, P.J., Darbyshire, D.P.F., and Greenwood, P.B., 2001, Petrogenesis of high Ba-Sr granites: The Rogart pluton, Sutherland: Geological Society of London Journal, v. 158, p. 521–534, doi:10.1144/jgs.158.3.521.

Fowler, M.B., Kocks, H., Darbyshire, D.P.F., and Greenwood, P.B., 2008, Petrogenesis of high Ba-Sr plutons from the Northern Highland Terrane of the British Caledonian Province: Lithos, 105, 129–148. doi:10.1016/j.lithos.2008.03.003.

Frost B.R., Barnes C.G., Collins W.J., Arculus R.J., Ellis D.J., Frost C.D. 2001. A geochemical classification for granitic rocks. Journal of Petrology, 42, 2033-2048. DOI: 10.1093/petrology/42.11.2033

Gerdes A., Zeh A. 2009. Zircon formation versus zircon alteration – New Insights from combined U-Pb and LuHf in-situ LA-ICP-MS analyses, and consequences for the interpretation of Archean zircon from the Central Zone of the Limpopo Belt. Chemical Geology, 261:230-243.

Goswami, B., Bhattacharyya, C., 2014. Petrogenesis of shoshonitic granitoids, eastern India: Implications for the late Grenvillian post-collisional magmatism. Geoscience Frontiers, 5, 821-843.

Grossi-Sad J.H., Lobato L.M., Pedrosa-Soares A.C., Soares Filho B.S. 1997. Projeto Espinhaço em CD-ROM (textos, mapas e anexos). Belo Horizonte, COMIG, 2693 p.

Guimarães M.L.V., Crocco-Rodrigues F.A., Abreu F.R., Belo de Oliveira O.A., Greco F.M. 1993. Geologia do Bloco Itacambira-Monte Azul entre Barrocão e Porteirinha (MG). In: Simpósio Nacional De Estudos Tectônicos, 4, Belo Horizonte. Resumos... Belo Horizonte, Sociedade Brasileira de Geologia, p. 74-78 (in Portuguese).

Hawkesworth, C.J., Cawood, P.A., Kemp, A.I.S., Storey, C.D., Dhuime, B., 2009. A matter of preservation. Science 323, 49–50

Hayden, L.A., Watson, E.B., Wark, D.A., 2008. A thermobarometer for sphene (titanite). Contributions to Mineralogy and Petrology 155, 529-540.

Heaman, L.M., 2009. The application of U-Pb geochronology to mafic, ultramafic and alkaline rocks: an evaluation of three mineral standards. Chem. Geol. 261 (1–2), 42–51.

Heilbron, M., Cordani, U.G., Alkmim, F.F., 2017. The São Francisco Craton and its margins. In: Heilbron, M., Cordani, U.G., Alkmim, F.F. (eds.). São Francisco Craton, eastern Brazil: tectonic genealogy of a miniature continent. New York, NY: Springer Berlin Heidelberg; 2017.

Heilbron, M., Duarte, B.P., Valeriano, C.M., Simonetti, A., Machado, N., Nogueira, J.R., 2010. Evolution of reworked Paleoproterozoic basement rocks within the Ribeira belt (Neoproterozoic), SE-Brazil, based on U/Pb geochronology: Implications for paleogeographic reconstructions of the São Francisco-Congo paleocontinent. Precambrian Research, 178: 136-148.

Heilimo, E., Halla, J., Hölttä, P., 2010. Discrimination and origin of the sanukitoid series: Geochemical constraints from the Neoarchean western Karelian Province (Finland). Lithos 115, 27–39.

Jackson, S.E., Pearson, N.J., Griffin, W.L., Belousova, E.A., 2004. The application of laser ablation-inductively coupled plasma-mass spectrometry to in situ U–Pb zircon geochronology. Chemical Geology, 211, 47-69. https://doi.org/10.1016/j.chemgeo.2004.06.017

Janousek V., Farrow C.M., Erban V. 2006. Interpretation of whole-rock geochemical data in igneous geochemistry: introducing Geochemical Data Toolkit (GCDkit). Journal of Petrology, 47(6):1255-1259. https://doi.org/10.1093/petrology/egl013

Jiang, Y.H., Jiang, S.Y., Ling, H.F., Dai, B.Z., 2006. Low-degree melting of a metasomatized lithospheric mantle for the origin of Cenozoic Yulong monzogranite-porphyry, east Tibet: Geochemical and Sr–Nd–Pb–Hf isotopic constraints. Earth and Planetary Science Letters, 241, 617-633.

Jiang, Y.H., Jiang, S.Y., Ling, H.F., Zhou, X.R., Rui, X.J., Yang, W.Z., 2002. Petrology and geochemistry of shoshonitic plutons from the western Kunlun orogenic belt, northwestern Xinjiang, China: implications for granitoid geneses. Lithos, 63, 165-187.

Jiang, Y.H., Liu, Z., Jia, R.Y., Liao, S.Y., Zhou, Q., Zhao, P., 2012. Miocene potassic granite–syenite association in western Tibetan Plateau: Implications for shoshonitic and high Ba–Sr granite genesis. Lithos, 134-135, 146-162.

Knauer L.G., Silva L.L, Souza F.B.B., Silva L.R., Carmo R.C. 2007. Folha Monte Azul, SD.23-Z-D-II, 1:100.000. Belo Horizonte, UFMG/CPRM. 72 p (in Portuguese).

Knauer, L. G., Fantinel, L. M., Romano, A. W., Pereira, D. F. L. C., Boa, T. F. 2015. Folha Rio Verde Pequeno, escala 1:100.000. In: Pedrosa-Soares, A. C., Voll, E., Profeta , L. (Coord.). Projeto Fronteiras de Minas Gerais. CODEMIG/UFMG, Belo Horizonte, 51p (in Portuguese.

Labanieh, S., Chauvel, C., Germa, A., Martinique, X.Q., 2012. A Clear Case for Sediment Melting and Slab Dehydration as a Function of Distance to the Trench, Journal of Petrology, 53(12): 2441–2464.

Lara, P., Oyhantçabal, P., Dadd, K., 2017. Post-collisional, Late Neoproterozoic, high-Ba-Sr granitic magmatism from the Dom Feliciano Belt and its Cratonic foreland, Uruguay: Petrography, geochemistry, geochronology, and tectonic implications. Lithos, 277, 178-198.

Laurent, O., Martin, H., Doucelance, R.,Moyen, J.-F., Paquette, J.-L., 2011. Geochemistry and petrogenesis of high-K “sanukitoids” from the Bulai pluton, Central

Limpopo Belt, South Africa: implications for geodynamic changes at the Archean–Proterozoic boundary. Lithos, 123, 73–91.

Laurent, O., Martin, H., Moyen, J.-F., Doucelance, R., 2014. The diversity and evolution of late-Archean granites: Evidence for the onset of a “modern-style” platetectonics between 3.0 and 2.5 Ga. Lithos, 205, 208-235. DOI: 10.1016/j.lithos.2014.06.012

Lobato, L.M., 1985. Metamorphism, Metasomatism and Mineralization at Lagoa Real, Bahia, Brazil. Ph.D. thesis. The University of Western Ontario, London, Canada.

Lobato, L.M., Pimentel, M.M., Cruz, S.C.P., Machado, N., Noce, C.M., Alkmim, F.F., 2015. U-Pb geochronology of the Lagoa Real uranium district, Brazil: Implications for the age of the uranium mineralization. Journal of South American Earth Science, 58, 129-140.

Lopes, G.A.C., 2002. Projeto Guajeru, 1. CBPM, Salvador, p. 408.

Ludwig K.R. 2003. User’s Manual for Isoplot/Ex, Version 3.0, A geochronological toolkit for Microsoft Excel. Berkeley Geochronology Center Special Publication, 4, 73p.

Magalhães, J.R., Pedrosa-Soares, A.C., Pinheiro, M.A., Silva, L.C., Knauer, L.G., Bouvier, A., Baumgartner, L., 2018. First Lu-Hf, δ^{18}O and trace elements in zircon signatures from the Statherian Espinhaço anorogenic province (Eastern Brazil): geotectonic implications of a silicic large igneous province. Brazilian Journal of Geology, 48(4), 735-759.

Marschall, H., Schumacher, J.C., 2012. Arc magmas sourced from mélange diapirs in subduction zones. Nature Geoscience, 5(12):862-867.

Martin H., Moyen J.F., Rapp R.P. 2009. The sanukitoid series: magmatism at the Archean–Proterozoic transition. Earth Environmental Science Transactions of the Royal Society of Edinburgh, 100(1-2):15-33. https://doi.org/10.1017/S1755691009016120

Meen, J.K., 1990. Negative Ce anomalies in Archean amphibolites and Laramide granitoids, southwestern Montana, U.S.A. Chemical Geology, 81, 191–207.

Meert, J.G., Santosh, M., 2017. The Columbia supercontinent revisited. Gondwana Research, 50, 67-83.

Miller, C.F., Stoddard, E.F., Bradfish, L.J., Dollase, W.A., 1981. Composition of plutonic muscovite; genetic implications. Canadian Mineralogist, 19, 25–34.

Moreira, H., 2017. Caracterização petrológica, geoquímica e geocronológica de corpos intrusivos máficos da porção central da Serra do Espinhaço. Universidade Federal de Ouro Preto, Ouro Preto, Unpublished MsC Thesis.

Moreira H., Seixas L., Storey C., Fowler M., Lasalle S., Stevenson R., Lana C. 2018. Evolution of Siderian juvenile crust to Rhyacian high Ba-Sr magmatism in the Mineiro Belt, southern São Francisco Craton. Geoscience Frontiers, 4:977-995.

Morel, M.L.A., Nebel, O., Nebel-Jacobsen, Y.J., Miller, J.S., Vroon, P.Z., 2008. Hafnium isotope characterization of the GJ-1 zircon reference material by solution and laser-ablation MC-ICPMS. Chemical Geology, 255, 231-235.

Nasdala, L., Corfu, F., Valley, J.W., Spicuzza, M.J., Wu, F., LiQ., Yang, Y., Fisher, C., M€unker, C., Kennedy, A.K., Reiners, P.W., Kronz, A., Wiedenbeck, M., Wirth, R., Chanmuang, C.,Zeug, M., Vaczi, T., Norberg, N., H€ager, T., Kr€oner, A., Hofmeister, W., 2016. Zircon M127 – A homogeneous reference material forSIMS U-Pb geochronology combined with hafnium, oxy-gen and potentially, lithium isotope analysis. Geostandards and Geoanalytical Research, 40, 457–475.

Nebel, O., Munker, C., Nebel-Jacobsen, Y.J., Kleine, T., Mezger, K., Mortimer, N., 2007. Hf–Nd–Pb isotope evidence from Permian arc rocks for the long-term presence of the Indian–Pacific mantle boundary in the SW Pacific. Earth and Planetary Science Letters, 254, 377-392.

Nesbitt H.W., Young G.M. 1982. Early Proterozoic climates and plate motions inferred from major element chemistry of lutites. Nature, 299, 715-717. DOI: 10.1038/299715a0.

Noce C.M., Pedrosa-Soares A.C., Silva L.C., Armstrong R., Piuzana D. 2007. Evolution of polycyclic basement complexes in Araçuaí Orogen, based on U-Pb SHRIMP data: Implicatons for Brazil-Africa links in Paleoproterozoic time. Precambrian Research, 159:60-78. https://doi.org/10.1016/j.precamres.2007.06.001

Novo, T.A., 2013. Caracterização do Complexo Pocrane, Magmatismo Básico Mesoproterozóico e Unidades Neoproterozóicas do Sistema Araçuaí–Ribeira, com Ênfase em Geocronologia U-Pb (SHRIMP e LA–ICP–MS). 193. Universidade Federal de Minas Gerais, Belo Horizonte, Unpublished PhD Thesis.

O'Connor J.T. 1965. A classification for quartz-rich igneous rocks based on feldspar ratios. Virginia: US Geological Survey Professional Paper B525, USGS, p. 79-84.

Ohta, T., Arai H. 2007. Statistical empirical index of weathering in igneous rocks: A new tool for evaluating the degree of weathering. Chemical Geology, 240, 280-297. DOI: 10.1016/j.chemgeo.2007.02.017

Patersson, A., Scherstén, A., Gerdes, A., 2018. Extensive reworking of Archaean crust within the Birimian terrane in Ghana as revealed by combined zircon U-Pb and Lu-Hf isotopes. Geoscience Frontiers, 8, 173-189.

Paton, C., Hellstrom, J., Paul, B., Woodhead, J., Hergt, J., 2011. Iolite: freeware for the visualisation and processing of mass spectrometric data. J. Anal. At. Spectrom. 26, 2508.

Pearce, J. A., Harris, N. W., Tindle, A. G., 1984. Trace element discrimination diagrams for the tectonic interpretation of granitic rocks. Journal of Petrology, 25, 956-983.

Pearce, J.A., 1982. Trace element characteristics of lavas from destructive plate margins. In: Thorp, R.S. (Ed.), Andesites. John Wiley, New York, pp. 525e548.

Pearce, J.A., 1996. Sources and settings of granitic rocks. Episodes 19, 120–125.

Pearce, J.A., Peate, D.W., 1995. Tectonic implications of the composition of volcanic arc magmas. Ann. Rev. Earth Planet. Sci. 23, 251-283.

Pedrosa-Soares, A.C., Alkmim, F.F., 2011. How many rifting events preceded the development of the Araçuaí - West Congo orogen?. Geonomos, 19: 244–251.

Pedrosa-Soares, A.C., Noce, C.M., Wiedemann, C.M., Pinto, C.P., 2001. The Araçuaí-West Congo orogen in Brazil: An overview of a confined orogen formed during Gondwanland assembly. Precambrian Research, 110: 307-323.

Peixoto E.I.N. 2017. Arquitetura e evolução tectono-metamórfica da Saliência do Rio Pardo, Orógeno Araçuaí, MG. PhD Thesis, Universidade Federal de Ouro Preto, Ouro Preto (in Portuguese with English abstract).

Pitcher, W.S., 1997. The nature and origin of granite. Chapman & Hall, London.

R.P. Rapp, E.B. Watson, 1995. Dehydration melting of metabasalt at 8–32 kbar: implications for continental growth and crust–mantle recycling. Journal of Petrology, 36, 891-931

Rapp, R.P., Shimizu, N., Norman, M.D., and Applegate, G.S., 1999, Reaction between slab–Derived melts and peridotite in the mantle wedge: Experimental constraints at 3.8 GPa: Chemical Geology, 160, 335–356. doi:10.1016/S0009-2541(99)00106-0

Rogers, J.J.W., Santosh, M., 2002. Configuration of Columbia, a Mesoproterozoic supercontinent. Gondwana Research, 5, 5–22.

Romano, R., Lana, C., Alkmim, F.F., Stevens, G.S., Armstrong, R., 2013. Stabilizationofthe southern portion of the São Francisco Craton, SE Brazil, through a long-livedperiod of potassic magmatism. Precambrian Research, 224, 143–159.

Rosa M.L.S., Conceição H., Paim M.M., Santos E.B., Alves da Silva F.C., Leahy G.A.S., Bastos Leal L.R. 1996. Magmatismo potássico/ultrapotássico pós a tardi-orogênico (associado a subducção) no oeste da Bahia: Batólito Monzo-Sienítico de Guanambi-Urandi e os Sienitos de Correntina. Geochimica Brasiliensis, 10(1): 27-42 (in Portuguese).

Rosa, M. L. S., 1999. Geologia, Geocronologia, Mineralogia, Litogeoquímica e Petrologia do Batólito Monzo-Sienítico Guanambi-Urandi (SW-Bahia). Instituto de Geociências da Universidade Federal da Bahia, Salvador, Unpublished PhD Thesis.

Santos M.M., Lana C., Scholz R., Buick I., Schmitz M.D., Kamo S.L., Gerdes A., Corfu F., Tapster S., Lancaster P., Storey C.D., Basei M.A.S., Tohver E., Alkmim A., Nalini H., Krambrock K., Fantini C., Wiedenbeck M. 2017. A New Appraisal of Sri Lankan BB Zircon as a Reference Material for LA-ICP-MS U-Pb Geochronology and Lu-Hf Isotope Tracing. Geostandards and Geoanalytical Research, 41(3):335-358.

Santos E.B., Rosa M.L.S., Conceição H., Macambira M.J.B., Scheller T., Paim M.M., Leahy G.A.S. 2000. Magmatismo alcalino-potássico paleoproterozoico no SW da Bahia e NE de Minas Gerais, Maciço do Estreito: Geologia, idade, petrografia e litogeoquímica. Geochimica Brasiliensis, 14 (2): 249-267.

Santos Pinto, M., Peucat, J.J., Martin, H., Sabate, P., 1998. Recycling of the Archean continental crust: the case study of the Gaviao Block, Bahia, Brazil. Journal of South American Earth Science, 11, 487-498.

Seixas, L.A.R., Bardintzeff, J.-M., Stevenson, R., Bonin, B., 2013. Petrology of the high-Mg tonalites and dioritic enclaves of the ca. 2130 Ma Alto Maranhão suite:evidence for a major juvenile crustal addition event during the Rhyacian orogenesis, Mineiro Belt, southeast Brazil. Precambrian Research, 238, 18-41.

Seixas, L.A.R., David, J., Stevenson, R., 2012. Geochemistry, Nd isotopes and U–Pbgeochronology of a 2350 Ma TTG suite, Minas Gerais, Brazil: implications forthe crustal evolution of the southern São Francisco Craton. Precambrian Research, 196–197, 61–80.

Sena V.H., Oliveira A.L.R., Chaves A.O., 2018. Petrologia das suítes paleoproterozoicas Paciência e Catolé da porção setentrional do domínio Porteirinha. Geonomos, 26(1):43-50 (in Portuguese with English abstract).

Silva L.C. da, Pedrosa-Soares A.C., Armstrong R., Pinto C.P., Magalhães J.T.R., Pinheiro M.A.P., Santos G.G. 2016. Disclosing the Paleoarchean to Ediacaran history of the São Francisco Craton basement: The Porteirinha domain (northern Araçuaí orogen, Brazil). Journal of South American Earth Sciences, 68:50-67. https://doi.org/10.1016/j.jsames.2015.12.002

Silva, A.M., Chemale Jr., F., Heaman L., 1995. The Ibirité Gabbro and the Borrachudos granite – The rift related magmatism of mesoproterozoic age in the Quadrilátero Ferrífero (MG). In: SBG, Simp. Geol. de Minas Gerais, 8, Belo Horizonte, Anais, 1, 89-90.

Silva, L.C. da., Armstrong, R., Noce, C.M., Carneiro, M.A., Pimentel, M.M., PedrosaSoares, A.C., Leite, C.A., Vieira, V.S., Silva, M.A., Paes, V.J.C., Cardoso Filho, J.M., 2002. Reavaliaçao da evoluç ão geologica em terrenos pr e-cambrianos brasi-leiros, com base em novos dados U-Pb SHRIMP, Parte II: orogeno Araçuaí, Cinturão mineiro e Craton Sao Francisco Meridional. Rev. Bras. Geociencias, 32 (4), 513-528 (in Portuguese with English abstract).

Silva, L.C. da., McNaughton, N.J., Armstrong, R., Hartmann, L.A.I., Fletcher, I.R., 2005. The neoproterozoic mantiqueira Province and its African connections: a zirconbased UePb geochronologic subdivision for the Basiliano/Pan-African systems of orogens. Precambrian Research, 136, 203-240.

Sláma, J., Kosler, J., Condon, D.J., Crowley, J.L., Gerdes, A., Hanchar, J.M., Horstwood, M.S.A., Morris, G.A., Nasdala, L., Norberg, N., Schaltegger, U., Schoene, B., Tubrett, M.N.,Whitehouse,M.J., 2008. Plesovice zircon – a new natural reference material for U–Pb and Hf isotopic microanalysis. Chemical Geology, 249, 1–35

Söderlund, U., Patchett, J.P., Vervoort, J.D., Isachsen, C.E., 2004. The ^{176}Lu decay constant determined by Lu-Hf and U-Pb isotope systematics of Precambrian mafic intrusions. Earth and Planetary Science Letters, 219, 311-324.

Spandler, C., Hammerli, J., Sha, P., Hilbert-Wolf, H., Hu, Y., Roberts, E. and Schmitz, M., 2016. MKED1: a new titanite standard for in situ analysis of Sm–Nd isotopes and U–Pb geochronology. Chemical Geology, 425.110-126.

Stacey, J.S., Kramers, J.D., 1975. Approximation of terrestrial lead isotope evolution by a two-stage model. Earth and Planetary Science Letters 26, 207-221.

Tarney, J., Jones, C.E., 1994. Trace element geochemistry of orogenic igneous rocks and crustal growth models. Journal of the Geological Society of London, 151, 855-868.

Teixeira W., Oliveira E.P., Marques L.S. 2017. Nature and Evolution of the Archean Crust of the São Francisco Craton. In: Heilbron M., Cordani U.G., Alkmim F.F. (Eds.). São Francisco Craton, Eastern Brazil: Tectonic Genealogy of a Miniature Continent. Switzerland, Springer International Publishing, p. 29-56.

Teixeira, W., Ávila, C. A., Dussin, I. A., Corrêa Neto, A. V., Bongiolo, E. M., Santos, J. O., Barbosa, N. S. (2015). A juvenile accretion episode (2.35–2.32 Ga) in the Mineiro belt and its role to the Minas accretionary orogeny: Zircon U–Pb–Hf andgeochemical evidences. Precambrian Research, 256, 148-169. https://doi.org/10.1016/j.precamres.2014.11.009

van Achterbergh, E., Ryan, C. G., Jackson, S. E., Griffin, W. (2001). Appendix III. Data reduction software for LAICP-MS. In: P. Sylvester (Ed.). Laser-ablation-ICP-MS in the Earth sciences, principles and applications. Mineralogical Association of Canada. Short Course Series, 29, 239-243.

Wang, W., Cawood, P.A., Zhou, M.F., Zhao, J.H., 2016. Paleoproterozoic magmatic and metamorphic events link Yangtze to northwest Laurentia in the Nuna supercontinent. Earth and Planetary Science Letters, 433, 269-279.

Whalen, J.B., Currie, K.L., Chappell, B.W., 1987. A-type granites: geochemical characteristics, discrimination and petrogenesis. Contributions to Mineralogy and Petrology, 95, 407-419. DOI: 10.1007/BF00402202

Woodhead, J.D., Hergt, J.M., 2005. A preliminary appraisal of seven natural zircon reference materials for in situ Hf isotope determination. Geostandards and Geoanalytical Research, 29, 183-195.

Wosniak, R., A.A.M.M, Oliveira, R.L.M., 2013. Mapa Geológico Folha Condeúba (1: 100,000). Serviço Geológico do Brasil (in Portuguese).

Wu, F.Y., Yang, Y.H., Xie, L.W., Yang, J.H., Xu, P., 2006. Hf isotopic compositions of the standard zircons and baddeleyites used in UePb geochronology. Chemical Geology, 234, 105-126.

Ye, H.M., Li, X.H., Li, Z.X., Zhang, C.L., 2008. Age and origin of high Ba–Sr appinite–granites at the northwestern margin of the Tibet plateau: implications for early

Paleozoic tectonic evolution of the Western Kunlun orogenic belt. Gondwana Research, 13, 126–138.

Zhao, G., Li, S., Sun, M., Wilde, S.A., 2011. Assembly, accretion, and break-up of the Palaeo-Mesoproterozoic Columbia supercontinent: record in the North China Craton revisited, International Geology Review, 53 (11-12), 1331-1356

Zhou, Z.X., 1986. The origin of intrusive mass in Fengshandong, Hubei Province. Acta Petrol. Sin. 2, 59–70 (in Chinese).

Figure captions:

Figure 1 – (A) Geotectonic contextualization of the São Francisco craton in the context of western Gondwana, highlighting the main Archaean nuclei (modified from Alkmim et al. 2006). (B) Simplified geological map of the São Francisco craton and Araçuaí orogen highlighting the Archaean and Paleoproterozoic assemblage refered as the São Francisco paleocontinent (modified from Cruz et al., 2016; Silva et al., 2016; Bersan et al., 2018). Archaean nuclei: 1 – Quadrilátero Ferrífero area; 2 – Gavião; 3 – Jequié; 4 – Serrinha; 5 – Itacambira-Monte Azul; 6 – Guanhães. Paleoproterozoic arcs: a – Mineiro belt (Minas orogeny); b – Mantiqueira Complex; c – Juiz de Fora Complex; d – Pocrane Complex; e – Western Bahia Magmatic Arc.

Figure 2 – Simplified geological map of the Itacambira-Monte Azul Block and southwestern Gavião nuclei (modified from Cruz et al., 2016 and Silva et al., 2016).

Figure 3 – Geological map of the study area (after Costa and Danderfer, 2017) with samples location.

Figure 4 – Field aspects and photomicrograficas showing textures and mineralogy of the Córrego Tinguí Complex granitoids (A–C) and Montezuma granitoids (D–O). (A) Field aspec of the samples T1A to T1C location. (B and C) Photomicrographs from granodiorites with anhedral plagioclase associated with quartz, biotite and wite-mica. Note that most of the plagioclase crystals are sericitized. (D and E) Higly foliated Montezuma granitoids with proto- to mylonitic texture. (F) Photomicrograph from sample T7A showing that the foliation is marked by the aligin of Biotite crystals, with K-feldspars and microcline being the main porfiroblasts. Quartz and plagioclase occur as small anhedral grains. (G and E) Field and thin-section aspect of the unfoliated granodioritic sample T3B, with secondary epidote associated with biotite. (I and J) Sligtly foliated outcrops from samples T5 and VM-82 respectively. (K) Thin-section from sample VM-82 showing larger crystals of alkali-feldspars and plagioclase with quartz and biotite constituting a fine grained matrix for these monzogranites. Note in the center of the image the presence of a euhedral titanite. In (L and M), note the large

euhedral to subhedral titanite crystals within the main mineralogy of sample VM-82. Note that these grains have no inclusions of Fe-Ti oxides. (N and O) Outcrop and thin-section aspect of a quart-monzonite from sample T2B. In (O), epidote occurs associated with biotite and most of the plagioclase shows a cloud aspect due to sericitization. Qtz – quartz; Mc – microcline; Kfs – K-feldspar; Pl – plagioclase; Bt – biotite; Wm – wite mica; Ttn – titanite; Ep – Epidote.

Figure 5 – Plots of mineral chemistry for feldspars (A), Biotite (B–E) and muscovite (F). See text for further explanations and references.

Figure 6 – Geochemical classification diagrams for Montezuma and Córrego Tinguí Complex granitoids (references in the text).

Figure 7 – Harker diagram for the Montezuma and Córrego Tinguí Complex granitoids.

Figure 8 – (A) Chondrite-normalized REE patterns. (B) Primitive mantle-normalized trace element spider diagram. Normalizing values for chondrite and primitive mantle are from Boynton (1984) and McDonough and Sun (1995), respectively.

Figure 9 – (A) Representative zircons CL images and $^{207}Pb/^{206}Pb$ weighted mean ages from sample VM-82. Note the complex structures and the inverse zoning in the ca. 1.8 Ga zircons. (B) Concordia diagram for LA-ICP-MS zircon and titanite U-Pb dating from sample VM-82. (C) Representative BSE-SEM images and Concordia age diagram of the analyzed titanite.

Figure 10 – Hf isotope data for zircons from sample VM-82. (A) $^{176}Hf/^{177}Hf_{(t)}$ vs. apparent $^{207}Pb/^{206}Pb$ date illustrating the three groups of zircon populations identified. (B) Plot of $\varepsilon_{Hf}(t)$ vs. U-Pb ages.

Figure 11 – Tectonic and geochemical discriminant diagrams from Montezuma and Córrego Tinguí Complex granitoids. (A and B) I, S and A-type granitoids diagram proposed by Whalen et al. (1987). (C) High Ba-Sr granitoids discrimination diagram after Tarney and Jones (1994). (D) Sr/Y vs. Y diagram after Drummond and Defants (1990). (E) Ternary classification diagram from Laurent et al. (2014). (F) Rb vs. Y+Nb diagram of Pearce et al. (1984); the post-collisional field is from Pearce (1996).

Figure 12 – (A–C) Ratios between fluid/melt-mobile and fluid/melt-immobile trace elements can be used to evaluate the importance of subduction fluids and/or sediment melts in the source metasomatism. Fields in (B) are after Laurent et al. (2011). (D) Pearce and Peate (1995) Th/Yb vs. Nb/Yb diagram with the boundary between felsic igneous rocks from oceanic and continental arcs from Condie and Kröner (2013).

Figure 13 – Schematic model for the evolution of magmatism and the generation of two contrasting groups of post-collisional shoshonitic high Ba-Sr granitoids within the northeastern sector of the São Francisco paleocontinent. See text for discussions. (A) Pre- to sin-collisional stage with two subduction zones with the same polarity being responsible for the contrasting nature of mantle metasomatism between the eastern and western sectors. (B) Post-collisional stage, where the processes of slab break-off and lithospheric delamination triggered the partial melting of the previously metasomitized lithospheric mantle. CC – Continental crust; OC – Oceanic crust; JC – Juvenile crust; SCLM – Subcontinental lithospheric mantle

Supplementary files captions:

Supplementary figure 1 – MFW (Mafic-Felsic-Weathering) diagram from Ohta and Arai (2007). For fields and equations used for M, F and W calculation, see Ohta and Arai (2007).

Supplementary figure 2 – Diagram of $^{207}Pb/^{206}Pb$ age versus ^{207}Pb and ^{206}Pb counts per second.

Supplementary figure 3 – Scanned thin-sections described in this study.

Supplementary table 1 – Mineral chemistry data.

Supplementary table 2 – Zircon LA-ICPMS U-Pb isotopic data.

Supplementary table 3 – Titanite LA-ICPMS U-Pb isotopic and trace elements data.

Supplementary table 4 – Zircon Lu-Hf isotopic data.

Sample	T7B	T7A	T3B	T5	VM82	T3A	T2B	T2C	T2A	T1A	T1C	T1B
Major element (wt.%)												
SiO_2	61.58	63.43	64.75	65.07	65.47	65.55	66.04	70.1	70.58	73.08	73.43	74.35
TiO_2	0.86	0.78	0.68	0.68	0.69	0.66	0.49	0.37	0.37	0.18	0.22	0.17
Al_2O_3	14.97	14.32	14.73	14.85	14.97	14.75	16.89	14.31	14.12	14.57	14.43	13.98
$Fe_2O_3{}^T$	5.71	5.52	4.66	4.55	4.38	4.59	2.75	2.56	2.51	1.45	1.58	1.34
MgO	3.44	3.21	2.2	1.85	1.83	2.41	0.94	0.68	0.9	0.53	0.39	0.35
MnO	0.07	0.08	0.07	0.07	0.07	0.06	0.03	0.04	0.04	0.02	0.02	0.02
CaO	2.1	2.24	2.84	2.33	2.65	2.09	1.25	1.48	1.37	1.09	1.51	1.33
Na_2O	3.2	2.91	3.4	3.29	3.41	3.26	3.97	3.58	3.75	4.54	4.35	4.12
K_2O	4.88	4.89	4.36	4.89	4.8	4.63	5.81	4.85	4.45	3.15	3.33	3.52
P_2O_5	0.37	0.35	0.21	0.26	0.25	0.21	0.12	0.11	0.1	0.03	0.06	0.05
LOI	1.07	0.95	0.61	0.75	1.09	0.83	0.67	1.07	0.92	0.58	0.43	0.45
Total	98.25	98.68	98.51	98.59	99.61	99.04	98.96	99.15	99.11	99.22	99.75	99.68
K_2O/Na_2O	1.53	1.68	1.28	1.49	1.41	1.42	1.46	1.35	1.19	0.69	0.77	0.85
CIA	51	50	49	50	49	51	53	51	51	53	52	52
A/CNK	1.04	1.01	0.95	0.99	0.96	1.04	1.12	1.03	1.05	1.13	1.07	1.07
$100\times Mg\#$	55	54	49	45	46	51	41	35	42	42	33	34
Rare earth and trace elements (ppm)												
Ba	2210	2357	1701	1925	1771	1924	1796	1287	1271	745	740	760
Be	5	2	3	<1	3	3	5	5	4	8	2	<1
Co	48.6	48.1	41.6	48.2	73.8	42.3	37.1	55.5	53.3	64.9	62.7	71.1
Cs	3.9	3.3	2.2	4.2	3.8	1.7	1.5	1.3	1	2.6	2.5	1.9
Ga	19.9	19.3	19.4	19.5	19	19.2	22.6	18.5	19.4	20.5	20.3	19.1
Hf	8.8	7.1	7.4	7.6	8.6	7.3	9.8	7.7	7.5	4.4	4.2	3.6
Nb	18.7	16.7	14.9	16.2	17	15	27.7	20.1	19.4	6	6.6	5.6
Rb	144.2	140.2	129.9	155.1	142.7	127	186.6	162.7	158	101.4	102.3	98.8
Sn	4	4	2	3	3	2	3	2	3	1	<1	<1
Sr	945.8	923.8	1022.8	951.9	985.6	759	515.3	469.4	374.2	140.2	170	159.1
Ta	1.8	1.8	1.2	2	2.1	1.5	2.5	2.3	2.1	0.9	0.8	1

Th	38.1	29.9	23	23.7	35.5	22.2	64	47.3	45.2	17	13.7	15.6
U	4.8	4.2	3	4.7	5.2	3.5	10	9.9	10.1	4.3	6.1	3.8
V	90	77	68	60	71	69	26	17	20	10	9	9
Zr	335	277.8	290	292.1	322.1	275.5	376.5	287.4	278.9	139.1	139.4	126
Y	33.7	27.3	30.8	27.2	44.4	24	26.4	25.3	23.1	5.3	4.8	5.1
La	221.1	128.5	122.7	102.5	271.1	61.1 (*100)	41.8	109.1	111.9	29.5	30	40.3
Ce	241.3 (*370)	184.8	167.4	189.6	192.6 (*380)	174.1	268 (*100)	202.7	199.1	60.3	48.4	63.3
Pr	41.59	21.87	21.48	21.39	40.14	13.29	10.34	20.01	20.16	6	6.14	7.73
Nd	147.5	78.9	74.5	75	136.2	49.2	34.5	66.8	66.3	20.8	21.8	27.5
Sm	20.84	11.94	11.56	11.54	19.99	8.68	6.77	10	10.11	4.21	3.66	4.47
Eu	4.56	2.98	2.34	2.78	4.15	1.71	1.16	1.51	1.51	0.57	0.64	0.7
Gd	14.11	9.55	8.99	8.55	16.05	7	6.12	7.93	7.17	3.2	2.75	3.62
Tb	1.6	1.15	1.09	1.12	1.92	0.93	0.88	0.95	0.87	0.37	0.34	0.4
Dy	7.16	5.41	5.7	6.05	9.44	4.74	5.18	4.81	4.24	1.49	1.38	1.51
Ho	1.29	0.97	0.95	0.96	1.58	0.91	0.92	0.83	0.79	0.19	0.21	0.19
Er	3.5	2.62	2.81	2.7	3.78	2.46	2.73	2.36	2.16	0.37	0.39	0.37
Tm	0.49	0.4	0.41	0.43	0.55	0.36	0.46	0.34	0.35	0.05	0.05	0.04
Yb	3.35	2.58	2.32	2.84	3.4	2.28	2.87	2.25	2.14	0.31	0.3	0.28
Lu	0.47	0.38	0.36	0.38	0.51	0.33	0.45	0.33	0.32	0.05	0.04	0.04
AI	0.7	0.7	0.7	0.72	0.72	0.7	0.76	0.78	0.78	0.75	0.75	0.76
ΣREE	708.86	452.05	422.61	425.84	701.41	327.09	382.18	429.92	427.12	127.41	116.1	150.45
Sr/Y	28	34	33	35	22	32	20	19	16	26	35	31
$(La/Yb)_N$	45	34	36	24	54	18	10	33	35	64	67	97
Eu/Eu*	0.82	0.86	0.71	0.86	0.71	0.67	0.55	0.52	0.55	0.48	0.62	0.53

Group	$^{207}Pb/^{206}Pb$ age (Ga)	$^{176}Hf/^{177}Hf_{(t)}$	$\varepsilon_{Hf}(t)$	T_{DM}^{2} (Ga)
I - inherited	2.25–2.04	0.2813249–0.2816689	–4.11 to +8.87	2.10–2.69
II - magmatic crystallization	2.04–1.90	0.2814430–0.2817241	–3.06 to +8.17	1.95–2.53
III - re-setting ages with inverse zoning	1.90–1.76	0.2816376–0.2817849	+0.46 to +5.48	1.93–2.21

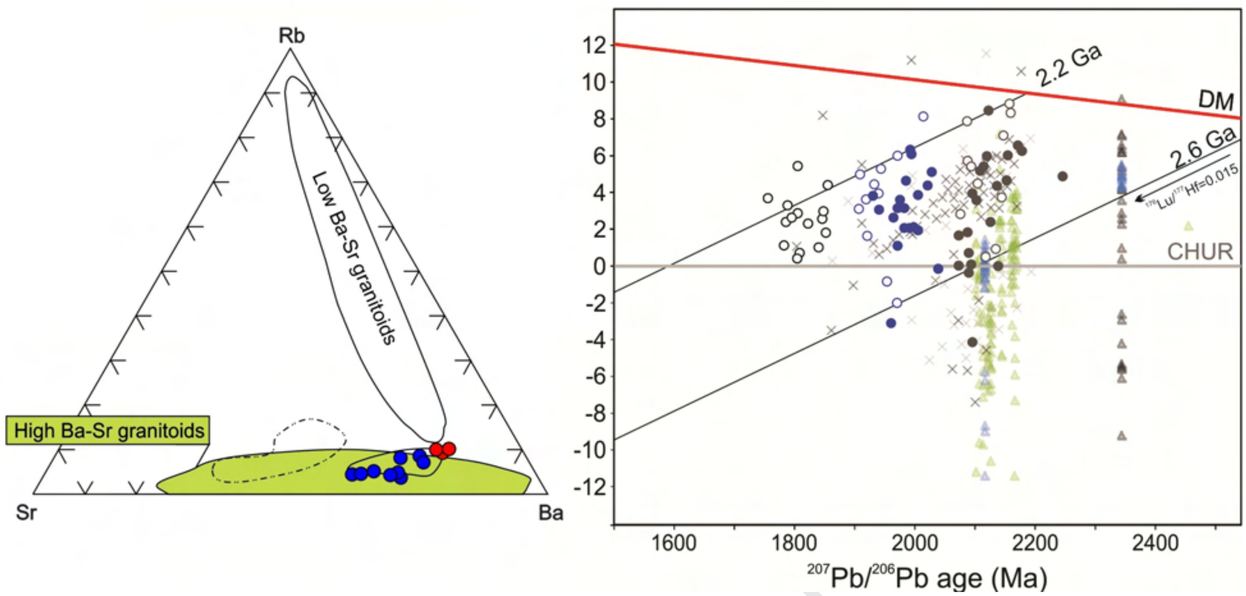
Rb
Sr
Ba
Low Ba-Sr granitoids
High Ba-Sr granitoids
2.2 Ga
DM
2.6 Ga
CHUR
12
10
8
6
4
2
0
-2
-4
-6
-8
-10
-12
1600
1800
2000
2200
2400
207Pb/206Pb age (Ma)

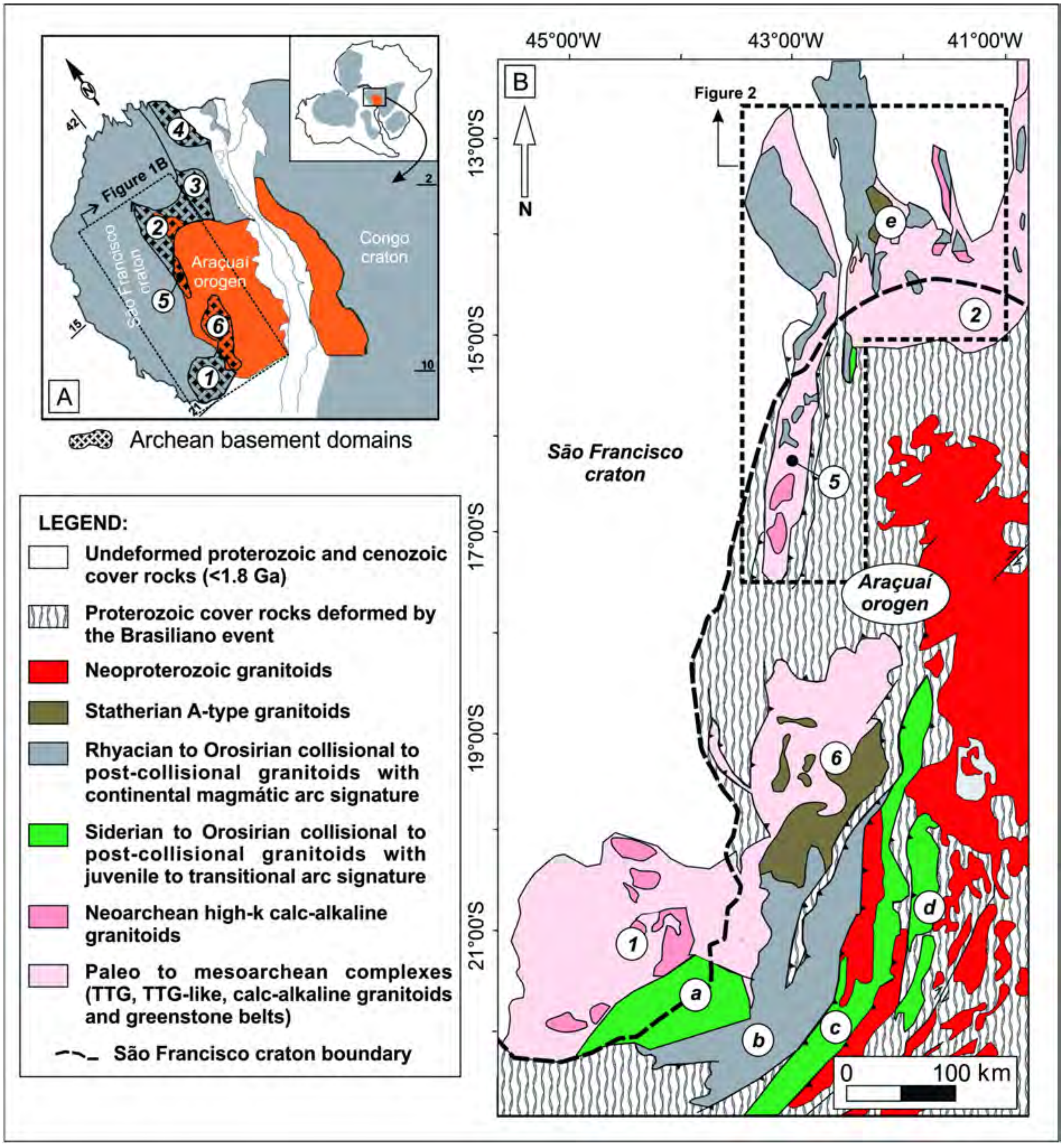

Figure 1B
São Francisco craton
Araçuaí orogen
Congo craton
A
Archean basement domains
LEGEND:
Undeformed proterozoic and cenozoic cover rocks (<1.8 Ga)
Proterozoic cover rocks deformed by the Brasiliano event
Neoproterozoic granitoids
Statherian A-type granitoids
Rhyacian to Orosirian collisional to post-collisional granitoids with continental magmátic arc signature
Siderian to Orosirian collisional to post-collisional granitoids with juvenile to transitional arc signature
Neoarchean high-k calc-alkaline granitoids
Paleo to mesoarchean complexes (TTG, TTG-like, calc-alkaline granitoids and greenstone belts)
São Francisco craton boundary
45°00'W
43°00'W
41°00'W
13°00'S
15°00'S
17°00'S
19°00'S
21°00'S
B
Figure 2
N
São Francisco craton
Araçuaí orogen
0
100 km

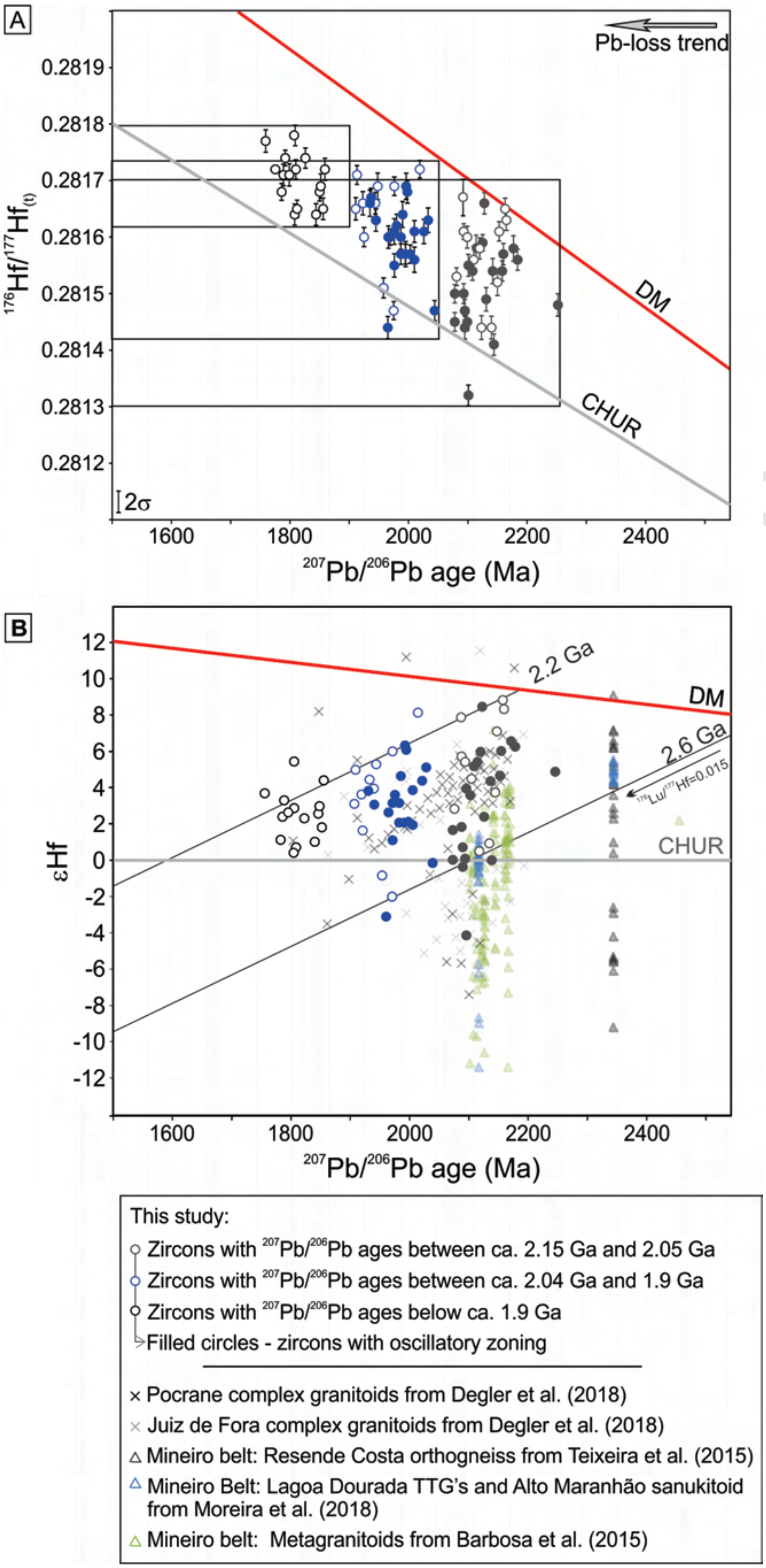
A
Pb-loss trend
0.2819
0.2818
0.2817
0.2816
0.2815
0.2814
0.2813
0.2812
176Hf/177Hf(t)
DM
CHUR
2σ
1600
1800
2000
2200
2400
207Pb/206Pb age (Ma)
B
12
10
8
6
4
2
0
-2
-4
-6
-8
-10
-12
εHf
2.2 Ga
DM
2.6 Ga
176Lu/177Hf=0.015
CHUR
1600
1800
2000
2200
2400
207Pb/206Pb age (Ma)
This study:
Zircons with 207Pb/206Pb ages between ca. 2.15 Ga and 2.05 Ga
Zircons with 207Pb/206Pb ages between ca. 2.04 Ga and 1.9 Ga
Zircons with 207Pb/206Pb ages below ca. 1.9 Ga
Filled circles - zircons with oscillatory zoning
Pocrane complex granitoids from Degler et al. (2018)
Juiz de Fora complex granitoids from Degler et al. (2018)
Mineiro belt: Resende Costa orthogneiss from Teixeira et al. (2015)
Mineiro Belt: Lagoa Dourada TTG's and Alto Maranhão sanukitoid from Moreira et al. (2018)
Mineiro belt: Metagranitoids from Barbosa et al. (2015)

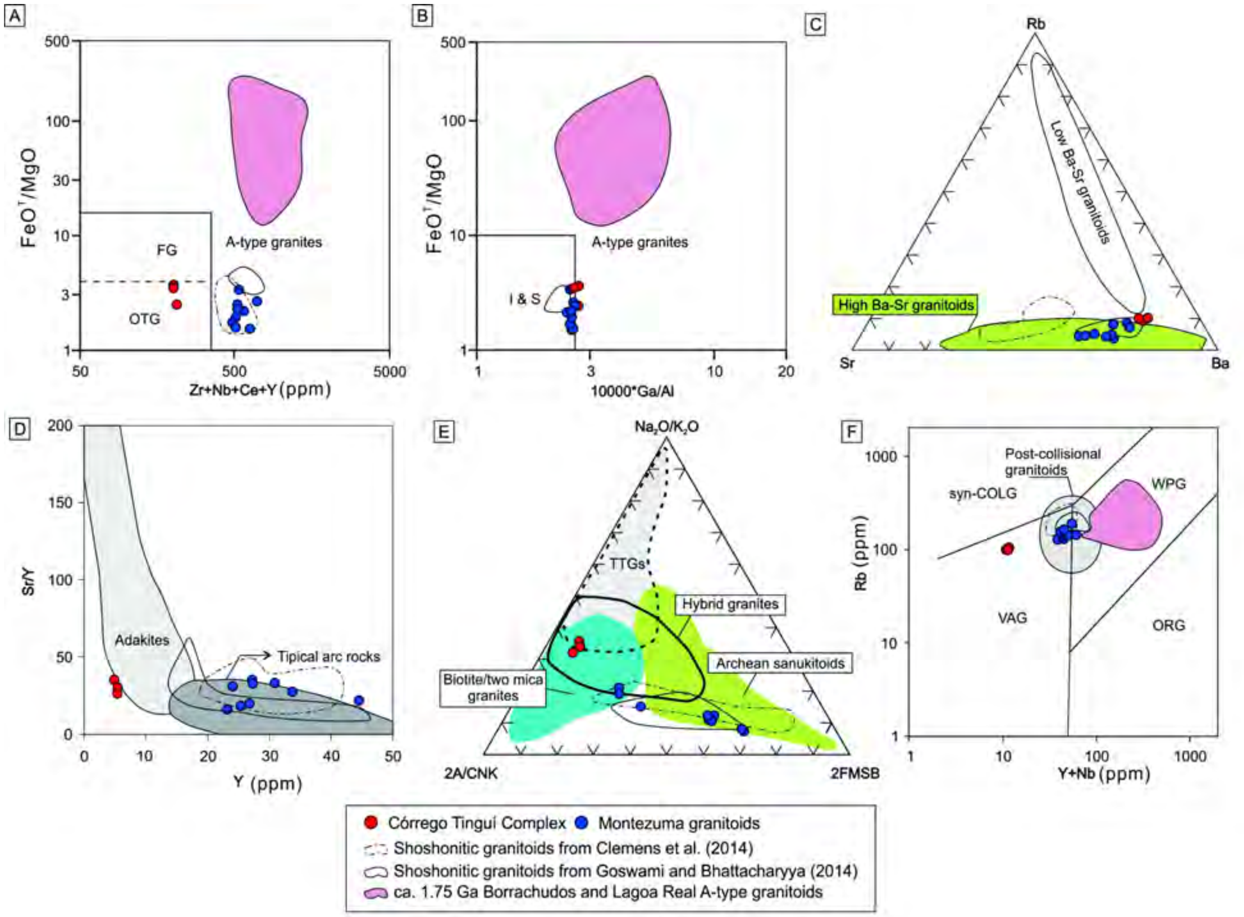

A
FeO^T/MgO
Zr+Nb+Ce+Y (ppm)
FG
OTG
A-type granites
B
10000*Ga/Al
I & S
A-type granites
C
Rb
Sr
Ba
Low Ba-Sr granitoids
High Ba-Sr granitoids
D
Sr/Y
Y (ppm)
Adakites
Tipical arc rocks
E
Na2O/K2O
2A/CNK
2FMSB
TTGs
Hybrid granites
Archean sanukitoids
Biotite/two mica granites
F
Rb (ppm)
Y+Nb (ppm)
Post-collisional granitoids
syn-COLG
WPG
VAG
ORG
Córrego Tinguí Complex
Montezuma granitoids
Shoshonitic granitoids from Clemens et al. (2014)
Shoshonitic granitoids from Goswami and Bhattacharyya (2014)
ca. 1.75 Ga Borrachudos and Lagoa Real A-type granitoids

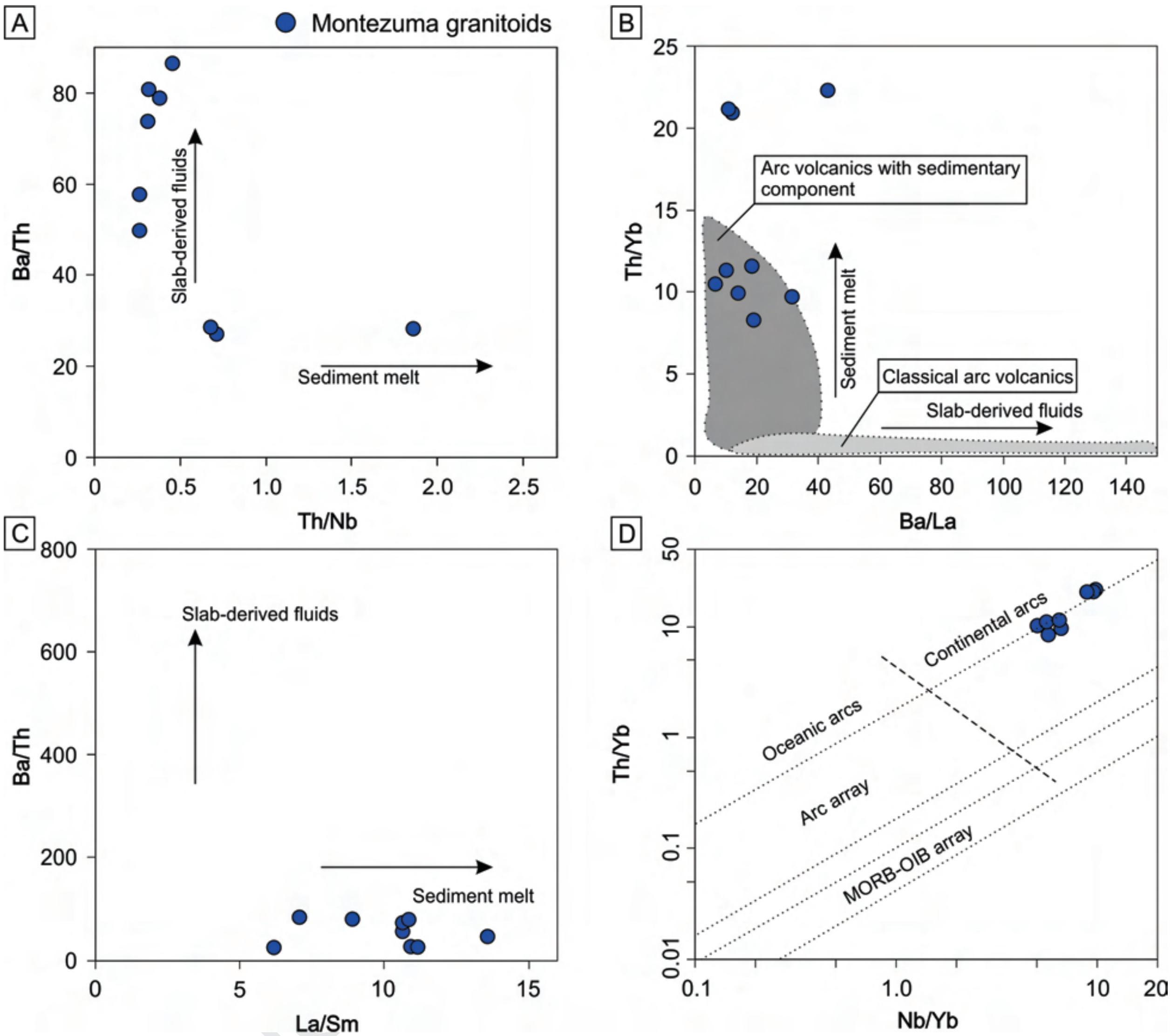
A
Montezuma granitoids
Ba/Th
Th/Nb
Slab-derived fluids
Sediment melt
B
Th/Yb
Ba/La
Arc volcanics with sedimentary component
Classical arc volcanics
Sediment melt
Slab-derived fluids
C
Ba/Th
La/Sm
Slab-derived fluids
Sediment melt
D
Th/Yb
Nb/Yb
Continental arcs
Oceanic arcs
Arc array
MORB-OIB array

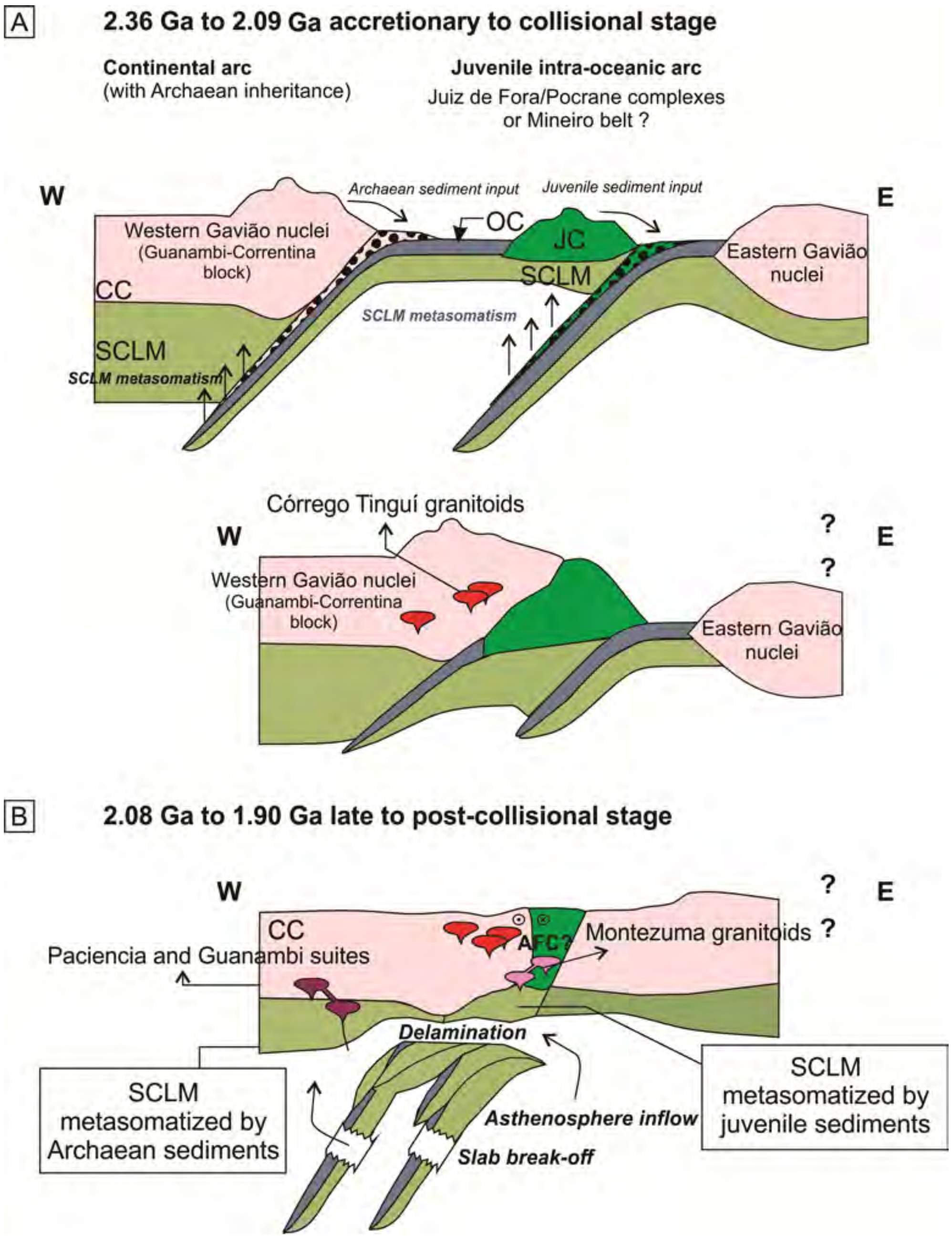
A
2.36 Ga to 2.09 Ga accretionary to collisional stage
Continental arc
(with Archaean inheritance)
Juvenile intra-oceanic arc
Juiz de Fora/Pocrane complexes
or Mineiro belt ?
W
Archaean sediment input
Juvenile sediment input
E
Western Gavião nuclei
(Guanambi-Correntina
block)
OC
JC
Eastern Gavião
nuclei
CC
SCLM
SCLM metasomatism
SCLM
SCLM metasomatism
Córrego Tinguí granitoids
W
?
E
?
Western Gavião nuclei
(Guanambi-Correntina
block)
Eastern Gavião
nuclei
B
2.08 Ga to 1.90 Ga late to post-collisional stage
W
?
E
CC
Montezuma granitoids
?
AFC?
Paciencia and Guanambi suites
Delamination
SCLM
metasomatized by
Archaean sediments
Asthenosphere inflow
Slab break-off
SCLM
metasomatized by
juvenile sediments

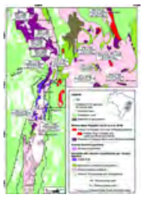

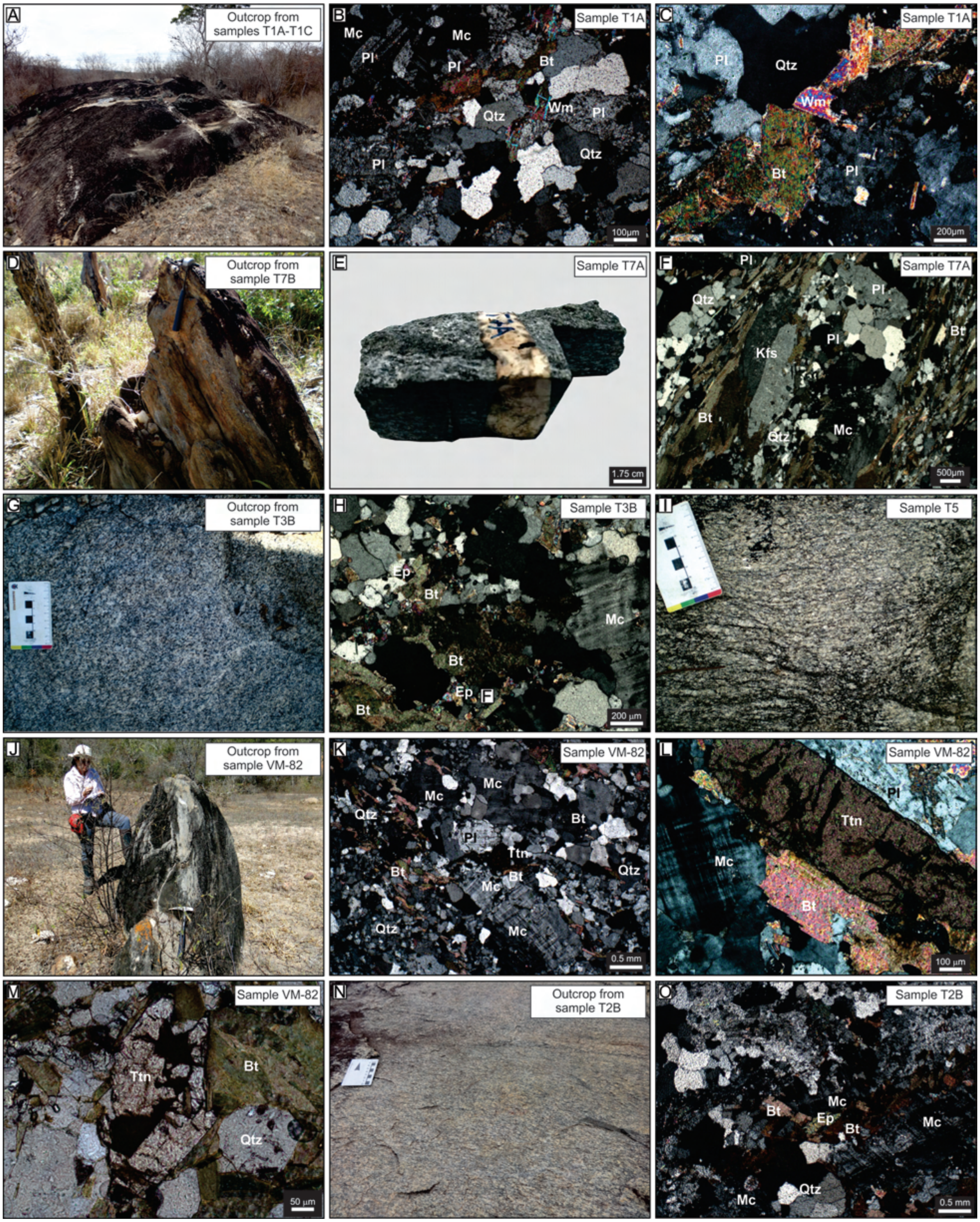
A
Outcrop from samples T1A-T1C
B
Sample T1A
Mc
Mc
Pl
Pl
Bt
Qtz
Wm
Pl
Pl
Qtz
100μm
C
Sample T1A
Pl
Qtz
Wm
Bt
Pl
200μm
D
Outcrop from sample T7B
E
Sample T7A
1.75 cm
F
Sample T7A
Pl
Qtz
Pl
Pl
Bt
Kfs
Bt
Qtz
Mc
500μm
G
Outcrop from sample T3B
H
Sample T3B
Ep
Bt
Mc
Bt
Ep
Bt
200 μm
I
Sample T5
J
Outcrop from sample VM-82
K
Sample VM-82
Mc
Mc
Qtz
Bt
Pl
Ttn
Qtz
Bt
Mc
Bt
Qtz
Mc
0.5 mm
L
Sample VM-82
Pl
Ttn
Mc
Bt
100 μm
M
Sample VM-82
Ttn
Bt
Qtz
50 μm
N
Outcrop from sample T2B
O
Sample T2B
Bt
Mc
Ep
Bt
Mc
Qtz
Mc
0.5 mm

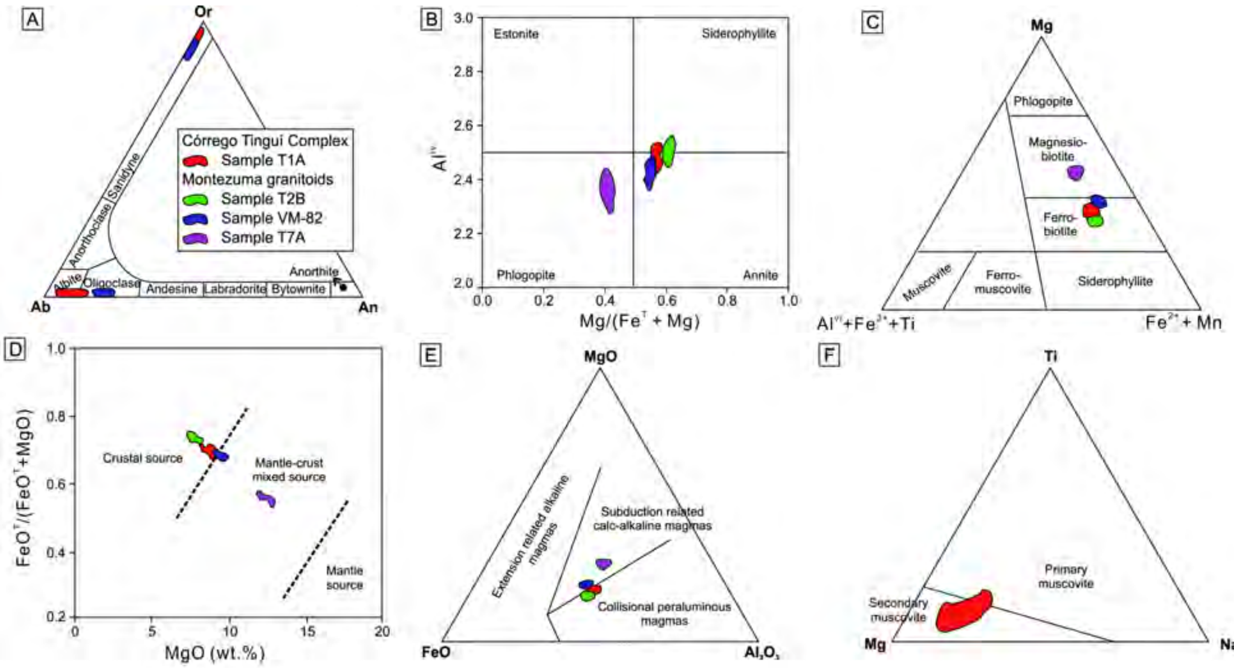
A
Or
Ab
An
Córrego Tinguí Complex
Sample T1A
Montezuma granitoids
Sample T2B
Sample VM-82
Sample T7A
Anorthoclase
Sanidyne
Albite
Oligoclase
Andesine
Labradorite
Bytownite
Anorthite
B
Estonite
Siderophyllite
Phlogopite
Annite
Al^{iv}
Mg/(Fe^{T} + Mg)
C
Mg
Phlogopite
Magnesio-biotite
Ferro-biotite
Muscovite
Ferro-muscovite
Siderophyllite
Al^{vi}+Fe^{3+}+Ti
Fe^{2+}+ Mn
D
Crustal source
Mantle-crust mixed source
Mantle source
FeO^{T}/(FeO^{T}+MgO)
MgO (wt.%)
E
MgO
FeO
Al_2O_3
Extension related alkaline magmas
Subduction related calc-alkaline magmas
Collisional peraluminous magmas
F
Ti
Mg
Na
Primary muscovite
Secondary muscovite

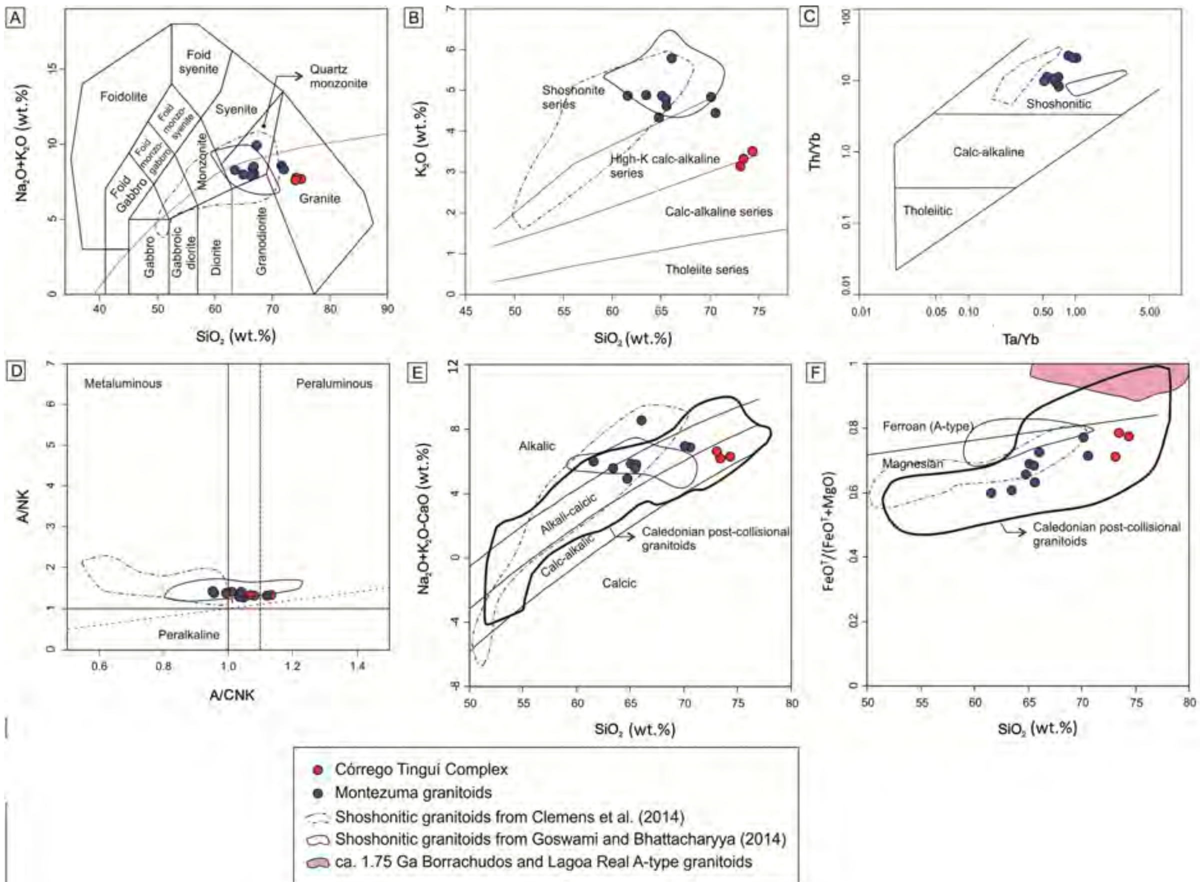
A
Foidolite
Foid syenite
Quartz monzonite
Syenite
Foid monzo-syenite
Foid monzo-gabbro
Foid Gabbro
Monzonite
Granite
Gabbro
Gabbroic diorite
Diorite
Granodiorite
Na_2O+K_2O (wt.%)
SiO_2 (wt.%)
B
Shoshonite series
High-K calc-alkaline series
Calc-alkaline series
Tholeiite series
K_2O (wt.%)
SiO_2 (wt.%)
C
Shoshonitic
Calc-alkaline
Tholeiitic
Th/Yb
Ta/Yb
D
Metaluminous
Peraluminous
Peralkaline
A/NK
A/CNK
E
Alkalic
Alkali-calcic
Calc-alkalic
Calcic
Caledonian post-collisional granitoids
Na_2O+K_2O-CaO (wt.%)
SiO_2 (wt.%)
F
Ferroan (A-type)
Magnesian
Caledonian post-collisional granitoids
$FeO^T/(FeO^T+MgO)$
SiO_2 (wt.%)
Córrego Tinguí Complex
Montezuma granitoids
Shoshonitic granitoids from Clemens et al. (2014)
Shoshonitic granitoids from Goswami and Bhattacharyya (2014)
ca. 1.75 Ga Borrachudos and Lagoa Real A-type granitoids

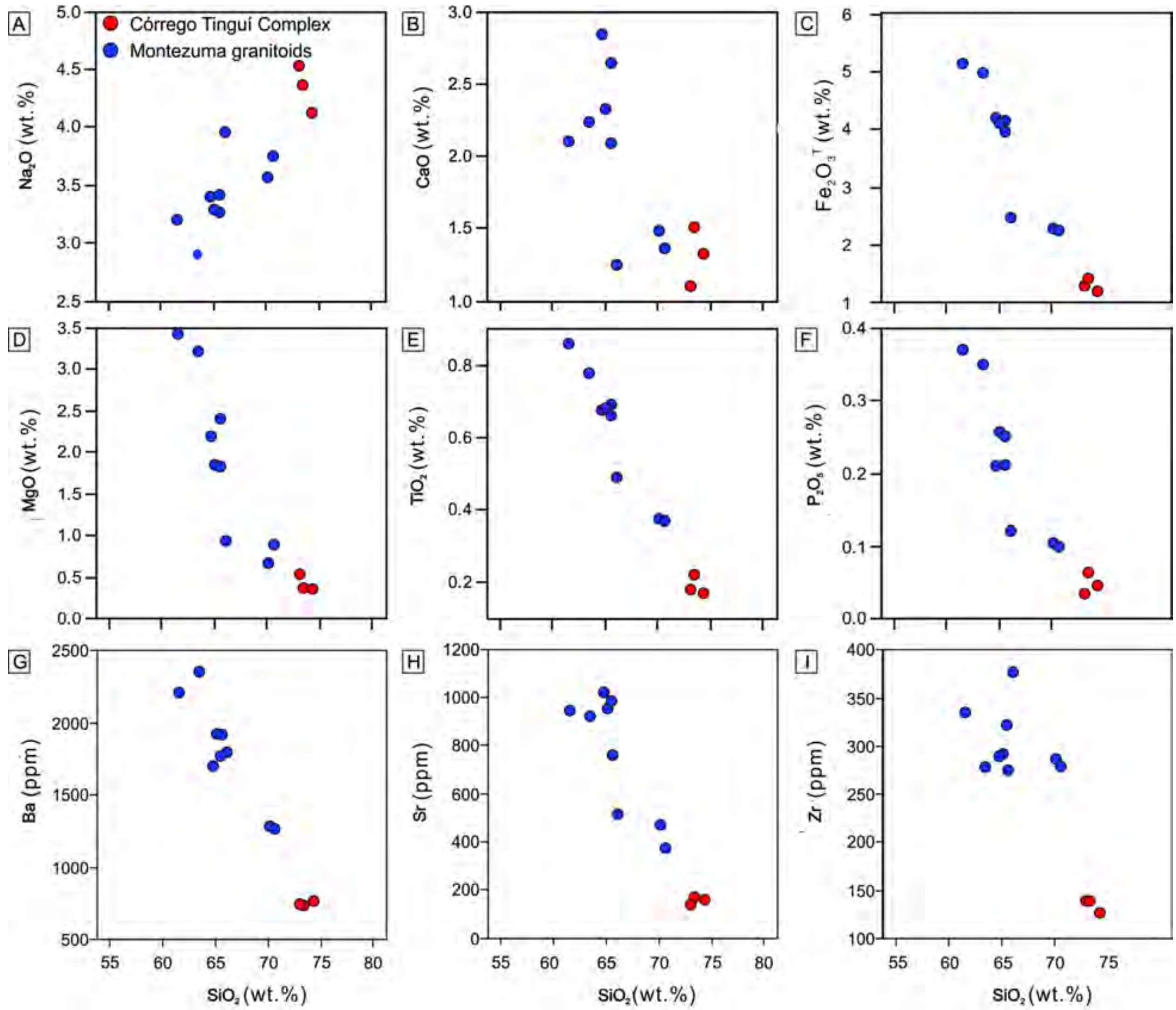
A
B
C
D
E
F
G
H
I
Córrego Tinguí Complex
Montezuma granitoids
Na2O (wt.%)
CaO (wt.%)
Fe2O3T (wt.%)
MgO (wt.%)
TiO2 (wt.%)
P2O5 (wt.%)
Ba (ppm)
Sr (ppm)
Zr (ppm)
SiO2 (wt.%)

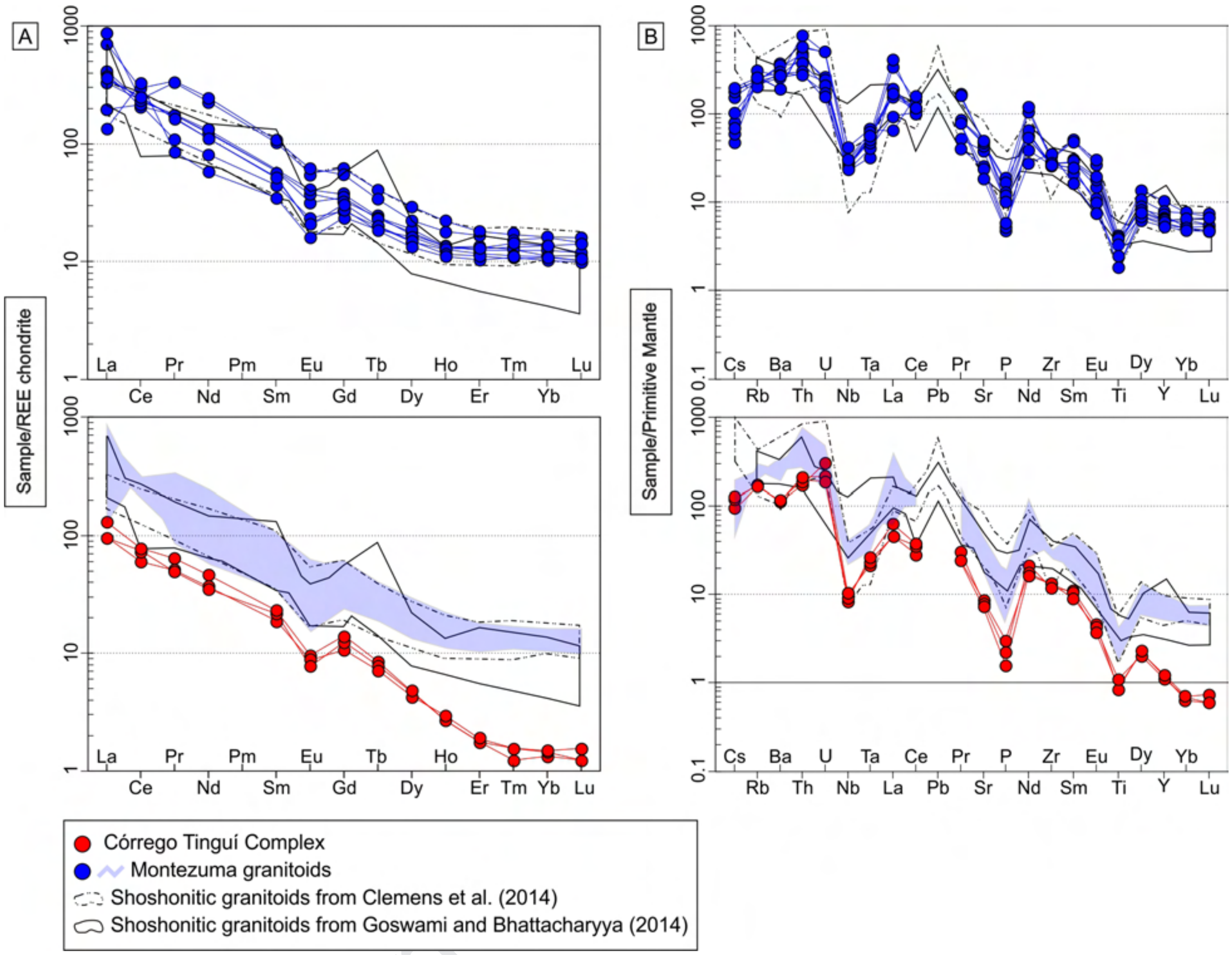
A
B
Sample/REE chondrite
Sample/Primitive Mantle
La Ce Pr Nd Pm Sm Eu Gd Tb Dy Ho Er Tm Yb Lu
Cs Rb Ba Th U Nb Ta La Ce Pb Pr Sr P Nd Zr Sm Eu Ti Dy Y Yb Lu
Córrego Tinguí Complex
Montezuma granitoids
Shoshonitic granitoids from Clemens et al. (2014)
Shoshonitic granitoids from Goswami and Bhattacharyya (2014)

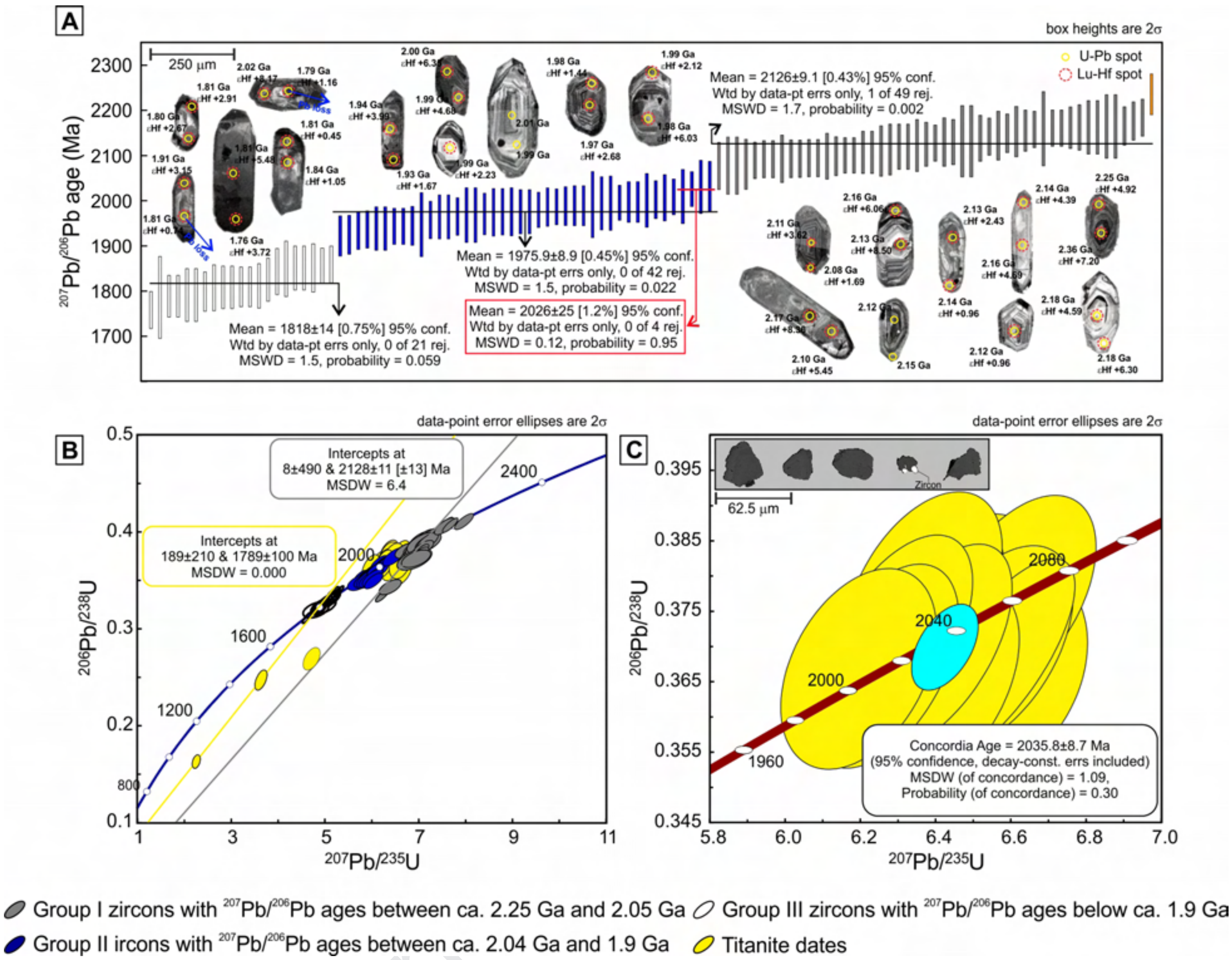
A
box heights are 2σ
U-Pb spot
Lu-Hf spot
250 μm
$^{207}Pb/^{206}Pb$ age (Ma)
Mean = 2126±9.1 [0.43%] 95% conf.
Wtd by data-pt errs only, 1 of 49 rej.
MSWD = 1.7, probability = 0.002
Mean = 1975.9±8.9 [0.45%] 95% conf.
Wtd by data-pt errs only, 0 of 42 rej.
MSWD = 1.5, probability = 0.022
Mean = 2026±25 [1.2%] 95% conf.
Wtd by data-pt errs only, 0 of 4 rej.
MSWD = 0.12, probability = 0.95
Mean = 1818±14 [0.75%] 95% conf.
Wtd by data-pt errs only, 0 of 21 rej.
MSWD = 1.5, probability = 0.059
B
data-point error ellipses are 2σ
Intercepts at
8±490 & 2128±11 [±13] Ma
MSDW = 6.4
Intercepts at
189±210 & 1789±100 Ma
MSDW = 0.000
$^{206}Pb/^{238}U$
$^{207}Pb/^{235}U$
C
data-point error ellipses are 2σ
62.5 μm
Zircon
Concordia Age = 2035.8±8.7 Ma
(95% confidence, decay-const. errs included)
MSDW (of concordance) = 1.09,
Probability (of concordance) = 0.30
Group I zircons with $^{207}Pb/^{206}Pb$ ages between ca. 2.25 Ga and 2.05 Ga
Group III zircons with $^{207}Pb/^{206}Pb$ ages below ca. 1.9 Ga
Group II ircons with $^{207}Pb/^{206}Pb$ ages between ca. 2.04 Ga and 1.9 Ga
Titanite dates

- Three zircon populations were obtained for the Montezuma granitoid.
- Titanite U-Pb age constrain the crystallization age of the Montezuma granitoid at ca. 2.03 Ga.
- Late- to post-collisional shoshonitic high Ba-Sr granitoid in the northeastern São Francisco paleocontinent.
- Lack of Archean inheritance and positive $\varepsilon_{\mathrm{Hf}}(t)$ signature.

Declaration of interests

☒ The authors declare that they have no known competing financial interests or personal relationships that could have appeared to influence the work reported in this paper.

☐The authors declare the following financial interests/personal relationships which may be considered as potential competing interests: